Articles   School of Electrical and Electronic Engineering

2024-11-14

Sustainable Mobility: Machine Learning-Driven Deployment of EV Charging Points in Dublin

Ruairí de Fréin
Technological University Dublin, ruairi.defrein@tudublin.ie

Alexander Mutiso Mutua Mr
Technological University Dublin

Follow this and additional works at: https://arrow.tudublin.ie/engscheleart2

Part of the Digital Communications and Networking Commons, Electrical and Electronics Commons, Power and Energy Commons, and the Systems and Communications Commons

Sustainable Mobility: Machine Learning-Driven Deployment of EV Charging Points in Dublin

Mutua, Alexander Mutiso and de Fréin, Ruairí

Technological University Dublin,
Ollscoil Teicneolaíochta Bhaile Átha Cliath,
Ireland
web: https://robustandscalable.wordpress.com

in: Sustainability. See also BIBTEX entry below.

Article

Sustainable Mobility: Machine Learning-Driven Deployment of EV Charging Points in Dublin

Alexander Mutiso Mutua [1],[†] (ID)**, Ruairí de Fréin** [2],[†],[*] (ID)

1 School of Electrical and Electronic Engineering, Technological University Dublin, Dublin, D07 EWV4, Ireland; d22124754@mytudublin.ie
2 School of Electrical and Electronic Engineering, Technological University Dublin, Dublin, D07 EWV4, Ireland; ruairi.defrein@tudublin.ie
* Correspondence: ruairi.defrein@tudublin.ie
† These authors contributed equally to this work.

Abstract: Electric vehicle (EV) drivers in urban areas face range anxiety due to the fear of running out of charge without timely access to charging points (CPs). The lack of sufficient numbers of CPs has hindered EV adoption and negatively impacted the progress of sustainable mobility. We propose a CP distribution algorithm that is machine learning-based and leverages population density, points of interest (POIs), and the most used roads as input parameters to determine the best locations for deploying CPs. The objects of the following research are as follows: (1) to allocate weights to the three parameters in a 6 km by 10 km grid size scenario in Dublin in Ireland so that the best CP distribution is obtained; (2) to use a feedforward neural network (FNNs) model to predict the best parameter weight combinations and the corresponding CPs. CP deployment solutions are classified as successful when an EV is located within 100 m of a CP at the end of a trip. We find that (1) integrating the GEECharge and EV Portacharge algorithms with FNNs optimises the distribution of CPs; (2) the normalised optimal weights for the population density, POIs, and most used road parameters determined by this approach result in approximately 109 CPs being allocated in Dublin; (3) resizing the grid from 6 km by 10 km to 10 km by 6 km and rotating it at an angle of $-350°$ results in a 5.7% rise in the overall number of CPs in Dublin; (4) reducing the grid cell size from 1 km^2 to 500 m^2 reduces the mean distance between CPs and the EVs. This research is vital to city planners as we show that city planners can use readily available data to generate these parameters for urban planning decisions that result in EV CP networks, which have increased efficiency. This will promote EV usage in urban transportation, leading to greater sustainability.

Keywords: electric vehicle charging points; charging infrastructure optimisation; charging point placement strategies; EV charging demand; machine learning; feedforward neural networks; sustainable urban planning; smart transport systems; range anxiety; optimisation of infrastructure

1. Introduction

Electric vehicles (EVs) have emerged as eco-friendly, with environmental and climate concerns taking centre stage in global climate action [1]. When powered by low-carbon electricity sources, such as renewable energy from micro-grid systems [2], EVs can contribute to reducing carbon emissions [3] and achieve economic decarbonisation targets [4–6]. Significant progress in energy research has driven the increased adoption of EVs. Raymond et al. [7] proposed the use of eco-friendly approaches to EV transportation. By adopting these approaches, societies can benefit and also contribute to achieving sustainability. Transport electrification is a route from renewable energy integration to support a zero-carbon economy. Renewable sources such as solar and wind depend on weather conditions, which affect the consistency of energy used in EV charging. Research in [8–10] focused on integrating renewable energy into EV charging systems and enhancing the

sustainability of vehicle-to-grid (V2G) operations. To facilitate transport electrification and meet the growing EV demand, research has concentrated on determining optimal sites for charging points (CPs). Researchers have formulated the problem of determining optimal locations for EV CPs using a variety of approaches, objective functions, and constraints. Advancements in battery technology and electric drive trains have positioned EVs as a viable solution for creating a sustainable transportation system [11]. EV industry growth will increase the demand for CPs, which will be strategically placed. Finding ideal locations for CPs is the main focus of current research.

The motivation behind this research stems from the urgent need to address range anxiety, a significant barrier to EV adoption caused by concerns about the availability of charging infrastructure. By optimising CP placement, we aim to enhance accessibility and convenience for EV drivers, ultimately supporting the broader transition to sustainable transportation. Two methods, namely, EV Portacharge and the green electric charge (GEECharge), are used to distribute CPs in Dublin. The EV Portacharge uses the approach outlined in [12] to assign scores based on POIs and population density. GEECharge expands this method by incorporating the most frequently used roads in each cell. When designing a method for CP distribution, it is essential to carefully consider factors such as population density, POIs, and road usage patterns. The parameters we choose are key since population density indicates potential demand volume, POIs signify areas where users are likely to stay for extended periods, and road usage identifies high-traffic routes prone to range anxiety. Despite the recent advancements in methods such as EV Portacharge and GEECharge, as discussed in [13], critical gaps and limitations still exist. This study focuses on Dublin, employing GEECharge distributed CPs. GEECharge integrates population density, POIs, and the most used roads parameters to ensure the efficient distribution of CPs. The research questions addressed by this research include the following:

- Which is the best method for identifying the most suitable location for CP placement?
- What factors play a role in determining the placement of CPs in urban areas?

The GEECharge method exhibits 2.2% higher efficiency compared to the EV Portacharge method, which only considers two parameters: population density and POIs. This research aims to deeply explore the complexities of CP distribution in Dublin, using GEECharge to address the following emerging issues and hypotheses:

H1: *There are parameters that influence the placement of CPs.*

H2: *There exist optimal weight parameter combinations that display a suitable number of CPs in a cell.*

H3: *Rotation and varying the size of the cell affects the CP distribution.*

H4: *Parameter scores and weights differ on different time scales.*

These hypotheses are built on gaps in the existing literature. Research in [14] discussed the significance of various urban parameters in determining the optimal placement of charging infrastructure. The spatial granularity of CP distribution models impacts their effectiveness, and rotating the grid could cover areas which were previously uncovered, and this could influence the distribution of CPs. Parameter scores and weights differ across time scales, hence the need to explore how this affects CP distribution.

This research builds upon the previous GEECharge CP distribution research in [13], addressing gaps in the existing literature and providing the following contributions:

- We use the GEECharge method to optimise the distribution of CPs in Dublin.
- We increase CP coverage by 5.7% when we resize the grid from 6 km by 10 km to 10 km by 6 km and rotate it at an angle of $-350°$.
- We integrate FNNs in CP distribution and establish that 109 is the optimal number in a 1 km^2 area.

- We reduce range anxiety by distributing CPs, thus reducing EV distance to a CP.
- We determine CP distribution efficiency in Dublin.

A driver should consider several factors when driving to recharge an EV. The factors include the EV's remaining range and CP availability. Keeping a battery charge between 10% and 20% is recommended due to concerns such as range anxiety, battery degradation [15,16], and delays that may extend the planned route. According to the authors in [17], 10% of global energy usage is attributed to ICT and network consumption. EVs deliver better performance and produce no tailpipe emissions, as discussed in [18]. To reduce carbon emissions and conserve energy, numerous countries are prioritising the development of the EV industry [19,20].

Table 1 shows statistics on the EV market. Due to the increase in uptake of EVs globally, the demand for public CPs has also increased. Research by Morrow et al. [21] found that the cost of EV transport systems can be reduced by increasing the number of CPs instead of increasing the size of batteries.

Table 1. Comparison of EV market statistics.

Statistic	Value	Source
US EV revenue (2024)	USD 82.8 Billion	[22,23]
US EV CAGR (2024–2028)	18.20%	[23]
US EV sales (2028)	2.46 Million units	[22,23]
Global EV revenue (2023)	USD 457.6 Billion	[24]
Global EV CAGR (2023–2027)	17.02 %	[24]
Global EV market volume (2027)	USD 858.0 Billion	[24]
Global EV sales (2027)	16.21 Million units	[24,25]
Average EV price (2023)	USD 53.2 Thousand	[24]
China's EV revenue (2023)	USD 190.4 Billion	[22,24]

The compound annual growth rate (CAGR) is a measure for determining the mean annual growth rate of an investment over a specified period longer than one year. We use it to show the growth of the EV market. The establishment of easily accessible CPs is a critical factor in the adoption of electro-mobility [13]. The absence of such infrastructure and EVs' relatively high cost and short range are significant obstacles to EV adoption [26,27]. The availability of CPs is one of the factors accelerating the electrification of road transportation. Studies outline challenges in closing gaps in CP availability to hasten the electrification of light-duty vehicles. One-third of greenhouse gas emissions in urban areas comes from these cars, which are utilised for light freight services as well as private and shared mobility, as proposed in [28]. It has been investigated and questioned whether investments in CPs are financially viable [29,30], particularly about rapid CPs.

Governments have worked on policies to accelerate the adoption of EVs, but integrating these EVs into our daily lives is still challenging [31]. Outside CPs can be helpful to EV owners even if they can charge EVs at home. This is due to battery charge degradation, as this limitation allows them to travel for a few hundred km [32]. For drivers to feel comfortable purchasing an EV, widely available CPs are required. Urban development efforts to address CP placement are limited by range anxiety [33–36]. CPs must be positioned well so that EVs can access one within driving range and easily navigate the city after recharging. Integrating the infrastructure for EV CPs into existing gasoline solutions may not be suitable. Traditionally, gasoline stations are primarily for petroleum refuelling, and adding EV infrastructure will overcrowd the minimal area available. Ireland has been installing CPs; however, drivers are concerned about CP accessibility. CPs must be easily accessible for everybody without disrupting or congesting the traffic. CPs should be placed

along the shortest paths, according to research in [37,38]. This paper builds upon the GEECharge method described in [13]. We make sure EVs have easy access to CPs.

Using a case study in Dublin, the GEECharge technique is tested in situations where an EV needs to charge when its position is approximately 100 m from CP access. The basis for employing a 100 m threshold is the cell size. A cell of 1 km^2 size is suitable since it ensures that all areas are comprehensively covered and CPs are efficiently distributed. This criterion ensures that CPs are easily accessible and close enough to one another to provide effective charging without necessitating long diversions. The rationale for using 100 m is also based on the idea that another CP could feasibly be reached with minimal additional travel in cases where one CP is busy. The 100 m distance supports quick roadside assistance and reduces the risk of EVs being stranded far from available CPs.

The structure of this research work is as follows. Section 2 explores the CP distribution literature. Section 3 describes how GEECharge and EV Portacharge are integrated in Dublin, utilising parameter weight analysis and CP distribution efficiency. In section 4, we discuss the evaluation of GEECharge and the parameter weights. Section 5 presents the GEECharge weight analysis. Section 6 presents recommendations for future work.

2. EV Charging Infrastructure Literature

Cities are adopting green developments as part of sustainability. EVs are increasingly being adopted as green transportation with very high energy efficiency, low pollution, and zero gas emissions. However, we have an increasing need for CP placement, and different methods and factors have been considered to solve the problem.

Population distribution: The placement of EV CPs is considered a multi-criteria problem, as discussed in [39,40]. Some approaches used population information for spatial partitioning and CP placement. Researchers in [14] examined the following CP distribution optimisation methods.

- *Random distribution approach (RDA):* A random allocation process is used by the RDA as a baseline against other distributions. This method involves placing EVs randomly across a map. While this method is straightforward, it does not consider factors like traffic density or other economic considerations.
- *Uniform distribution approach (UDA):* The UDA divides the map into square cells and places CPs evenly across the cells. The UDA attempts to provide balanced CP distribution based on the selected area. The method might be inefficient in areas with varying densities.
- *Concentric radial approach (CRA):* The CRA divided the map into triangular cells from a central point to form concentric circles. The CRA provides a focal point that centralises CPs around high-activity areas.
- *Genetic algorithm distribution (GAD):* GAD integrates multiple data sources to provide cell scores. Several factors such as population size, CP costs, and twitter activity are taken into account.

The researchers surrounded POIs using Voronoi polygons. Cells with higher scores were probable to receive a CP. In population data, the criterion involved analysing population density information in the selected area, ensuring that the EV-driving population could easily access the CP. This method's drawback is the unrealistic distribution of CP estimates. The multi-criteria approach in [12] used the population distribution sustainability factor as a constraint. CPs on roads located in areas with a large population were deemed suitable, as they would serve a greater number of people.

Square cells were created from the area, and each cell was assigned a score based on appropriateness factors. If a constraint was met, the cell's constraint score was set to 0; if not, it was set to 1. The sum of weighted appropriateness criteria multiplied by a constraint score was calculated as the final score. The manual selection of weights was carried out. This method was different from the research in [14], as scores were assigned to each cell based on a variety of variables. The authors in [35] developed an approach where

a population agent gathered information about people living in a particular area for EV CP placement. Areas that are densely populated often correlate with very high traffic volumes.

Twitter activity: The genetic algorithm in [14] also used geo-located tweets to act as a proxy for human activity patterns. These data were utilised to ascertain the locations where a given population spent time. This identified hot spots where demand for EV CPs would increase in the future, although the current usage data may not justify a need for CP placement.

Traffic information: Building on population data, traffic information plays a critical role in CP location. Researchers analysed traffic density and mobility patterns to optimise CP placement. The genetic algorithm in [14] incorporated traffic flow data and identified high-traffic routes and areas. A grid partitioning technique was proposed in [41]. The technique utilised genetic algorithms considering traffic density and CP capacity constraints [41]. The research used a case study of 48 intersections, 110 road sections, and an area of 63 km^2. The initial grid partition did not use traffic density information. The optimal CP placement in the partition was selected after the area was zoned using the partition approach. This allowed for consideration of CP capacity limits such as charging power, chargers per CP, and traffic density. The research routine focused on minimising the cost for EV users to access CPs.

The activity-based micro-simulation model (ActBM) discussed in [42] was used to simulate everyday movements and locations of EVs in the Flanders region of Belgium. ActBM determined how many EVs will run out of power and need to be recharged during the day based on the assumption that they all have fully charged batteries when they wake up. To ascertain the optimal site and timing for charging at the lowest possible cost, an optimisation algorithm was employed that took into account the fluctuating cost of power and the unique mobility patterns of each EV. The study calculated Flanders' overall electricity use and showed the regions that experienced the most traffic during rush hour. It looked at EV owners' activities while their vehicles were charging [42]. A genetic method was employed in [35]'s study technique to optimise the position of CPs. A multi-agent system (MAS) was the method suggested in [35] and examined various configurations for the positioning of CPs. The MAS integrated information from heterogeneous sources to provide the characteristics of where CPs could be potentially placed, as described in [35]. The method used a traffic agent to obtain traffic data. The technique tried to disperse the necessary CPs over the city and looked up potential CP sites. These methods ensured that the CP location selected used population data and actual traffic patterns, which are similar to the approaches in mobile sensing, looking to load-balance sensing across different communications access technologies over mobile handsets [43,44].

CP features: The focus of recent research has shifted towards the development of CP features that meet the diverse and time-varying EV users' demands. A multi-objective planning model-based numerical technique was developed for the CP layout in [45] by considering EV sustainable development, characteristics of CPs, and characteristics of users. The model in [45] was developed to be expandable as the EV sector is growing. A simulation of the model was carried out in Chengdu. Fabiano et al. [46] developed a structure for analysing and expanding public CPs. The model developed grouped CPs based on their profiles. The framework was for expanding public CPs due to the quick adoption of EVs. The model developed analysed data to model the CP electricity profile. This approach had the limitation of the assumption that EV distribution is proportional to market distribution in public CPs. After analysing the power model of CP infrastructure, the model grouped CPs with similar profiles. Other research was based on simulation to find a suitable site for CPs. Research in [47] developed a simulation optimisation model to locate public CPs to maximise EV service. A simulation optimisation model for the location of public electric vehicle charging infrastructure to maximise EV service was developed in [47]. The research used a sensitivity analysis modelling approach that considered each candidate location independently and demonstrated that a level-one and level-two combination of

slow charging technologies is better than level two [47]. Level-one charging operates at a lower voltage, resulting in a slower charging speed than level-two charging.

Infrastructure of the power grid: To understand the impact of CP infrastructure complexity on distribution, integration with the power grid is essential. The method in [45] took into account the power grid in the CP layout. Three distinct approaches were proposed to optimise EV CP locations and impact networks. Research by Fareed et al. [48] first proposed the distribution of network operators (DNO). The massive number of EVs challenges the DNO responsible for electric power provision due to the optimisation of power loss, bus voltages, and reliability [48]. Hyeon et al. [49] used stochastic second-order conic programming, which made a difference in optimising the measuring of conveyed generator units and EV CPs. The method considered vulnerabilities in framework resources through scenario-based stochastic programming. The integration of scenario-based stochastic programming provided a robust system for optimising conveyed generator units and EV CPs. In [49], the distribution planning process sufficiently determined the ideal sizing of distributed generator units and CPs. Yuvaraj et al. [50] investigated optimisation strategies to attain ideal outcomes, taking into account the effects of EV CP load in the distribution system (DS) as well as the economic and environmental consequences. The research employed the cuckoo search algorithm (CSA) and the bald eagle search algorithm (BESA) [50] to determine which energy sources were the best. Integrating CPs within the power grid enhances reliability and sets the stage for the strategic placement of CPs along the road networks.

Road characteristics: A multi-agent-based planning approach was proposed in [51] to optimise EV charging infrastructure on highways. The method assessed travel and charging activities on highways. This aimed to capture how drivers interact with EV CPs. The model helped evaluate the effectiveness of EV CP planning. The model facilitated comparing different planning mechanisms for allocating CPs on the highway, such as the dispersed, centralised, and mixed strategies [51]. The model assisted in determining the best course of action to maximise EV users' service level while preserving cost-effectiveness. The model aimed at expanding the CP network as the number of EVs increases, contributing to the sustainable integration of EVs into the transport system [51]. Researchers in [52] proposed to model the CP positioning problem in road networks on reachability graphs in Dublin and Boston [52]. Looking at CP placement along highways, it is also important to consider the existing infrastructure, such as petrol stations, as this can influence decisions on where to place CPs.

Presence of petrol stations: Due to existing gas station utilisation and demand priority, the solution in [45] was created. The researchers argued that a vacant place for CP construction should be found if a gas station is unavailable. In [12], multi-criteria approach roads near petrol stations were preferred for CP positioning. This was mainly for hybrid cars [12]. The authors in [53] described a mixed-integer mathematical model to optimise CP placement. The method used eligible points like existing petrol stations and other areas such as commercial centres and parking lots. The researchers also used historical petrol sales data to calculate the need for EV charging. This model limitation was the assumption that petrol sales data were representative of electric demand [53].

Renewable energy integration and the Internet of things (IoT): The transition from conventional fuelling methods to renewable energy has been gaining momentum. In [54], a creative and eco-friendly wireless EV charging approach incorporating renewable energy and Internet of things integration was created. The method majorly addressed a reliance on cable connections and CP options that are constrained [54]. The researchers designed a technology that can be used in the parking lots of offices. For EVs, the system enabled a cost-effective and sustainable energy source [54]. They offered a solution that allows for updates on CP slot availability. As the CP infrastructure evolves so fast, there is a need to address the pervasive issue of range anxiety among EV users.

Range anxiety mitigation: According to [55], customers' range anxiety and distance deviations were taken into consideration when studying the CP locating problem. The

authors employed an iterative greedy heuristic model, an adaptive large-neighborhood search, and a k-shortest path algorithm. The PROMETHEE method in [56] aimed to address the uncertainty of multi-criteria decision-making (MCDM) methods. The method integrated PROMETHEE and analytic network process (ANP) [56]. This research formulated EV CP placement and proved that it is non-deterministic polynomial-time challenging in CP placement, as illustrated in [57]. The placement of CPs also involves considering the economic aspects of the installation to address financial sustainability.

Cost of CPs: The second approach in [48] was the charge station owner (CSO) approach, which looked at all costs incurred while putting up and operating a CP. These costs included installation costs, waiting time costs, access costs, operating costs, and penalty costs. The final approach was to use an EV user, which optimised travelling, charging, and waiting time costs [48]. Cost models and genetic algorithms were used for the location optimisation of EV CPs [58]. The social cost model consisted of economic and environmental costs calculated for CP's operating cost. The genetic algorithm generated the population randomly for optimisation. This approach had the limitation of not fully expressing the constraints of optimisation. Evolutionary algorithms were developed to determine the best sites for infrastructure related to charging, as proposed in [59]. Their strategy was based on conservation theory, which assumed EVs inside the district as a CP's fixed load. The total amount and EV distribution were forecasted, and the CP minimal cost was proposed. Research by Frade et al. [60] was designed to maximise demand using a maximal coverage approach and was applied in Lisbon as a case study. To find the best location for CPs, predictive modelling was used, taking into account variables including energy and ports in CPs [61]. Mehmet et al. [39] presented a fuzzy multi-criteria decision analysis (MCDA) method. The method was based on GIS for placing CPs. A fuzzy analytical hierarchy process (AHP) and a technique for order preference by similarity to ideal solution (TOPSIS) approaches were used to identify possible CP locations in Ankara, Turkey.

The authors in [62] proposed a regression model and mixed integer programming (MIP) to locate CPs. Ordinary least squares (OLS) regression models predicted parking demand variables such as the parked time per vehicle trip. The MIP was modelled to minimise total access costs for EV users to CPs. To avoid clustering and budget constraints, the model ensured a minimum distance between CPs. The major limitation of this research was the presumption that demand for parking is a reliable indicator of demand for EV charging [62]. The researchers in [63] employed a bi-level optimisation approach integrating transportation and energy demands to locate and size CPs. The method considered existing CPs and aimed to minimise net costs. Links with CPs were duplicated to account for travel with and without recharging. The proposed model was applied in Genoa, Italy, as a case study, as described in [63]. The limitation of this research is that solving the bi-level optimisation problem can be computationally expensive.

A multi-objective site selection of electric CPs was proposed in [64] and aimed at simultaneously maximising system benefits and the minimum coverage level. POIs were clustered into functional areas using a combined clustering algorithm. The cluster centres were determined as charging demand points. The research determined the demand in the research area for each charging demand point, fitted the charging likelihood of different functional zones, as shown in [64], and examined the charging habits and travel patterns of electric car owners. To match the real area that the CP covers, the authors considered the CP's progressive coverage and introduced the NSGA-II algorithm [64]. Multi-objective optimisation was performed by maximising the minimal coverage level and maximising system benefits as the optimisation objectives. We now shift from CP cost optimisation to technological innovation in CPs.

Technology in EV charging: As discussed in [65], the power on the go solution was created to overcome EV charging difficulties. The authors proposed a way for EVs to be charged in convenient places. A service vehicle was dispatched from a nearby CP and delivered a suitable power bank upon the driver's request via an application [65]. The goal was to shorten the total amount of time that passes between service requests and the

beginning of charges. For both situations, the researchers offered heuristic techniques based on order-first split-second and formal formulations [65]. The order-first stage included the first order of elements, which was EV generation. In the split stage, the ordered sequence was divided into feasible solutions that adhered to the problem's constraints. For the EV charging problem, this meant assigning drones to the ordered sequence of EVs while considering constraints like drone autonomy, travel distances, and charging times. The heuristics were quick and effective, with gaps of < 5% for a maximum of 20 node instances. At the same time, the mathematical formulas could produce optimal solutions for small cases in a fair period. A mathematical programming formulation for modelling the deployment of wireless charging lanes in road networks was suggested. This addressed the challenge of determining the most critical nodes for placing these lanes. To address different realistic scenarios, the authors built upon the basic formulation and conducted experiments using accurate geospatial data, providing practical insights into the optimal placement of wireless charging lanes [66]. The authors in [66] modelled the placement of wireless charging lanes as an integer programming problem. The model considered scenarios like road segments to allow the network analysis, including traversal times. The researchers assumed that the state of charge (SOC) changes proportionally with the energy consumed or gained during the traversing. The limitation of this paper is that the proposed model may be influenced by factors such as changes in traffic patterns, evolving technology, and the dynamic nature of urban environments [66]. Other research explored macro-level planning for national highways to allow for the strategic placement of CPs.

Highway segment lengths: An optimisation technique to determine the best places for CPs on national roads was proposed in [67]. The model was developed, and suitable locations for CPs were selected, as well as how many CPs were to be set up. This was to ensure that drivers on highways did not develop range anxiety. The key factors considered included the daily average number of vehicles, highway segment lengths, and future EV adoption forecasts, where estimates were made about the future number of EVs and EV range [67]. The research enhanced optimal CP placement by proposing strategic placements [67].

EV adoption forecast: Other models explored integrating the forecast of EV adoption and the usage patterns in planning models. Research by Sweda et al. [68] was able to determine household EV ownership trends and coordinate efforts to identify critical sites for additional CPs, with the Chicago region as a case study, as shown in [68]. An equilibrium modelling framework was proposed for the best allocation of public CPs for plug-in hybrid EVs in metropolitan areas [69]. Xiaohong et al. [70] developed a spatial and temporal method to obtain EV CPs. Most CP location issues are based on currently used heuristics and optimisation techniques. Worley et al. [71] used a vehicle routing problem (VRP) and structured the task of locating CPs and ideal EV routings as a discrete integer programming problem. The developed integer programming model determined the least cost of routes and CP locations and minimised the sum of travel costs for EVs [71]. The authors in [72] proposed a mixed integer linear programming approach (MILP) that incorporated the maximum flow model to optimise the placement and sizing of EV CPs. The model evaluated user satisfaction within a given CP by determining the maximum flow that can be accommodated. The maximum flow model was integrated into the MLP to make decisions on opening new CPs. The research limitation included an assumption that all CPs are built at the beginning.

Many existing studies primarily use deterministic models or heuristic methods without incorporating machine learning. For example, approaches like genetic algorithm distribution (GAD) in the literature integrate various data sources but do not utilise prediction models for CP distribution. Previous research relied on static site selection. We select and optimise parameter weights based on their significance in CP distribution. We adjust the grid size from 6 km by 10 km to 10 km by 6 km and rotate it at certain angles. We demonstrate how different grid configurations influence CP distribution. Previous research does not mention the size of sites where CPs will be placed.

Table 2 shows aspects of GEECharge that differ from the previous research. Marti et al. [14] focused on grid-based partitioning and did not address the effects of grid size and rotation on CP placement. Our empirical analysis demonstrates that rotating and reducing the grid size improves the mean proximity of CPs. In contrast to earlier studies as shown in Table 3 and Table 4, such as Wu et al. [51] and Alanazi et al. [61], which used heuristics, linear regression, and SVM for CP placement, our work integrates FNN. This offers better CP distribution.

Table 2. This table shows that GEECharge considers population density, POIs, and the most used roads and FNN to predict the suitable number of CPs in a cell.

GEECharge Aspect	Description
Factors considered	Population density, Points of Interest (POIs), Most used roads.
Normalisation	Weights are normalised and sum to 1.
Prediction method	FNN is utilised to predict the best normalised weight combinations and the corresponding CPs.
Impact	Improves CP distribution encouraging the use of EVs.

Table 3. Comparison of methods used in electric vehicle charging point distribution, including techniques, key features, population/city, and results.

Technique	Author	Method	Features	City/population	Results
Stochastic Second-Order Conic Programming	Woo et al. [49].	System Sizing Optimisation, K-means	$\min_u \sum_{ij \epsilon L} l_{jj} R_{ij} + \sum_{j \epsilon B} \left(V_{1,j} + V_{2,j}\right)$	Seoul, South Korea 9.42 M in 2022 [73]	Reduced power system losses and enhanced stability.
Multi-objective Planning Model	Wang et al. [45].	Optimisation and Simulation	Energy consumption model: $E(r) = \pi r^2 \cdot x \cdot v$, Vehicle flux and velocity: $v = \frac{Q}{f}$, $e(x,y) = e(x,y) - s\left(x,y,x_j,y_j\right)$	Chengdu, China 9.8 M [74]	45 gas stations, 90 public infrastructures.
Optimal Siting Based on Voronoi Diagram and Fuzzy-AHP	Tang et al. [40].	Site optimisation using Voronoi diagrams and Fuzzy-AHP	Fuzzy-AHP integration: $W = \sum w_i \cdot x_i$	Beijing, China 21.86 M [75]	$C = \mathbf{A} \cdot \mathbf{B} = (0.31, 0.39, 0.21, 0.10)$.
Grid Partition Method	Ge et al. [41].	Locating and sizing using grid partition and Genetic Algorithm	Minimise Total Loss: $H = h_1 + h_2$, where $h_1 = L_j \cdot p \cdot g$ and $h_2 = L_j \cdot k \cdot v$	Not Specified	102 CPs in 9 partitions.
Spatial and Temporal Plan	Dong et al. [70].	Shared Nearest Neighbour (SNN) Clustering, OD,Queuing Theory	Queuing time: $L_s = L_q + \frac{\lambda}{\mu_2} = \frac{(c\rho)^c \rho}{c!(1-\rho)^2} P_0 + \frac{\lambda}{\mu_2}$: SNN: $s_{ij} = \text{size}(NN(i) \cap NN(j)) \quad 1 \leq i,j \leq n, i \neq j : s_{ii} = 0$	Hainan Island 10.2 M [76]	Scenario 1 has 15 CPs, Scenario 2 has 18 CPs.
Cost Model and Genetic Algorithm	Zhou et al. [58]	Location optimisation	$F_1 = \sum_{j \in J} Cj \left[T(N_j) \frac{r_0 (1+r_0)^{n_{\text{year}}}}{(1+r_0)^{n_{\text{year}}} - 1} + Y(N_j) \right]$	Ireland 5 M [77]	670 CPs.
Multi-objective site selection	Zhang et al. [64].	NSGA-II, TF-IDF	$TF - IDF(w_i) = TF(d, w_i) * IDF(w_i)$, $F1 = \max \frac{\sum_i \sum_j w_i q_{ij} z_{ij}}{\sum_i \sum_j c_j x_i + \sum_j b_j r_j} \quad F2 = \max q'$	Hohhot, China 2.44 M [78]	143 clusters, 67 CPs, minimum coverage level > 59.4%.
Multi-Agent System (MAS)	Jordán et al. [35].	Genetic Algorithms	$V(C_i) = \sum \left(\omega_p a_{\text{population}} + \omega_{tr} a_{\text{traffic}} \right) - \left(\omega_a \text{cost area} + \omega_c \text{cost per charger} \right)$	Valencia, Spain $839,770$ [79]	Scenario 1: 40 Cps and scenario 2 : 42 CPs.
Agent-Based Decision Support	Sweda and Klabjan [68]	Agent-based modelling	$y(a,t) = \text{argmin}_{vinV(a)} \big[\text{Price}(v,t) + E[\text{FuelCost}(v,a,t)] - \text{GreenBonus}(v,a) - \text{SocialInfluence}(v,a,t) + \text{LongDistancePenalty}(v,a) + E \text{ InfrastructurePenalty}(v,a,t)] \big]$	Chicago land area 7.5 M[80]	Base 20 Cps and 10.50 mi, Prop 1 additional 70 CPs and 5.01 mi, Prop 2 additional 70 Cps and 4.37 mi.

Table 3. *Cont.*

Technique	Author	Method	Features	City/population	Results
multiple domination	Gargarin et al. [52]	k-dominating, sets, Heuristic optimisation	$\gamma_k(G) \leq \left(1 - \frac{\delta'}{b_{k-1}^{1/\delta'}(1+\delta')^{1+1/\delta'}}\right)n$, $\gamma_\alpha(G) \leq \left(1 - \frac{\delta}{d_\alpha^{1/\delta}(1+\delta)^{1+1/\delta}}\right)n$	Dublin 72,589 and Boston 675,647 [81, 82]	2 km distance: Boston mean 1.9, std 1.1 and Dublin mean 2.0, std 1.1.
Predictive modelling	Alanazi et al. [61].	Linear regression, SVM	$Y = \beta o + \beta 1 \times X1 + \beta 2 \times X2 + \epsilon$, $Y = w \times X + b + \epsilon$,	Texas, New York, California 90 M [83]	90% accuracy, 94% precision, Recall 89%, 91% F1-score.
Fuzzy Multi-Criteria Decision Analysis (MCDA)	Erbas et al. [39].	GIS-based MCDA using Fuzzy AHP and TOPSIS	Fuzzy AHP and TOPSIS integration: Score $= \sum_i (w_i \cdot \text{fuzzy score}_i)$	Ankara, Turkey 5.4 M [84]	Optimally identified and ranked EVCS locations.

Table 4. Comparison of methods used in electric vehicle charging point distribution, including techniques, key features, population/city, and results.

Technique	Author	Method	Features (Key Equations)	City/Population	Results
Multi-Criteria Decision Analysis using AHP and GIS	Mostafa Mahdy et al. [12].	Multi-Criteria Decision, Weighted Linear Combination (WLC)	suitability factors(x_1, x_2), $\sum x_i w_i =$ factor aggregation	Winchester, UK 50,000 [85]	Identified 44 suitable locations.
Park-based assignment method	Chen et al. [62].	Regression modelling, Mixed Integer Programming (MIP)	$\min \sum_{i,j} c_{ij} y_{ij}$	Seattle, Washington, 4741 households and 10,510 individuals	access cost of 0.69 mi, 79.9% parking demand accessed CP within 1 mile of Traffic Analysis Zones (TAZ).
Functional Data Analysis and Clustering	Fabiano Pallonetto et al. [46].	Functional K-means Clustering	$\text{Cong}(c) = \sum_{t=1}^{T} \sum_{l=1}^{T} \frac{G_{t,t+l}(c)}{F_{t,t+l}(c)}$, $P(t) = \sum_{n=1}^{M} P_n(t)$	Ireland 5 M [77]	verified OOC or OOS for more that 30%, increased CP occupancy time 1200 h to 1400 h.
Activity-Based Microsimulation	Jairo González et al. [42].	Optimisation Algorithm	Optimisation: $\min \text{Cost}(\text{Schedule}, \text{Load})$	Flanders, Belgium 6.06 m [86]	EV demand $1-5$ kWh, 81% of driver charge at night, Overloaded areas identified.
Multi-objective optimisation	Bersani et al. [53].	Mixed Integer Programming	$\min\left\{\sum_{i=1}^{N}(k_i y_i + h_i A_i) - G \sum_{i=1}^{N} A_i\right\}$	Savona, Liguria, Italy, 30 eligible locations for CPs, including 20 existing petrol stations	Maximum distance is 9.7 km, With G= 10, 6 CPs were selected, capturing 82% of the total demand.
Multi-criteria Decision Making	Wu et al. [56].	Greedy approach Chemical reaction optimisation	$f_j(a) = \left(\min(l_i), \left(\sum_{i=1}^{k} m_i\right)/k, \max(u_i)\right)$	Beijing, China 21.86 M [75]	A4 > A3 > A2 > A1. A4 > A2 > A3 > A1.
NP-hard	Lam et al. [57].	PROMOTHEE, ANP	$\min_{1 \leq i \leq n}\left(\inf_{x \in \Omega_1} \sum_{j=1}^{n} c_j x_j\right)$., $x_1 + x_2 \xrightarrow{\text{greedy}} x_1' + x_2'$.	Hong Kong 7.4 M [87]	Proves problem is non-deterministic polynomial-time hard.
Maximal Covering Model	Frade et al. [60].	mixed integer Optimisation	$\max \sum_{i \in I} y_i$, s.t. $d(i,j) \leq d_{\max} \forall j$	Lisbon, Portugal 3 M [88]	Scenario 1: 180 supply points and 29CPs and scenario 2: 324 supply points and 43 Cps.

3. GEECharge and EV Portacharge Integration in Dublin

This research focuses on improving CP distribution in Dublin. We investigate parameters that influence CP placement. Understanding these parameters helps ensure that CPs are conveniently located where they are needed most. We use discrete event simulation (DES) to model EV interactions with CPs. The simulation allows us to assess how many EVs will be within a reasonable distance of a CP when charging needs to occur. We cover

GEECharge and EV Portacharge implementation in CP distribution in graph G with a set of vertices V and edges E, where $G = (V, E)$. The set of vertices V is defined as follows:

$$V = \{v_1, v_2, v_3, \ldots, v_n, \ldots, v_N\}, \tag{1}$$

where v_n represents the nth vertex in the graph network, with $n = 1, 2, 3, \ldots, N$. The edges are defined as follows:

$$E = \{e_1, e_2, e_3, \ldots, e_m, \ldots, e_M\}, \tag{2}$$

where $e_m = \{v_i, v_j\}$ represents an edge between vertices v_i and v_j. A set of edges can be expressed as follows:

$$E = \{\{v_i, v_j\}, \{v_k, v_n\}, \ldots, \{v_m, v_p\}\}. \tag{3}$$

The location of the i-th vertex is given by $l(v_i)$, where $l(v_i) = (x_i, y_i)$, and x_i and y_i represent the latitude and longitude, respectively. Similarly, the location of the jth vertex is denoted as $l(v_j)$, where $l(v_j) = (x_j, y_j)$, with x_j and y_j representing the latitude and longitude.

Notations $N = |V|$ and $M = |E|$ represent the total number of vertices and edges, respectively. We source data from [89] and produce daily reports on cars detected within the network junctions. The dataset referenced in [89] is for all types of vehicles (petrol, diesel, etc.). We used the data for all vehicles as we felt that it was important to show traffic volumes in Dublin for all vehicle types and also to know the most used roads. Commonly utilised junctions correspond to nodes, and each edge e_m is assigned a capacity $c(e_m)$ and a weight $w(e_m)$, which reflect the maximum traffic flow and the length in m, respectively. We express the maximum traffic flow as follows:

$$c(e_m) \quad \text{for} \quad e_m \in E. \tag{4}$$

The edge length in m is expressed as follows:

$$w(e_m) \quad \text{for} \quad e_m \in E. \tag{5}$$

The number of EVs detected at an intersection v_i at time τ is represented by $f(v_i, \tau)$. We represent the number of cars identified each day as follows:

$$f(v_i, \tau) \quad \text{for} \quad v_i \in V \quad \text{and} \quad \tau \in \{\tau_1, \tau_2, \ldots, \tau_{24}\}. \tag{6}$$

We show a methodological flowchart of our research, as shown in Figure 1.

Figure 1 shows the key methods used. We use GEECharge as it uses w_t, w_p, and w_d to maximise the efficacy of CP placement. We gather population and traffic data. The integration of three different parameters allows for a more accurate representation of urban mobility patterns. We use parameter weight normalisation to ensure that there is equity in weight contribution in CP distribution. We use discrete event simulation for dynamic modelling of EV interaction with CPs. In CP distribution, the relationships among w_t, w_p, and w_d are inherently non-linear. FNNs can learn these relationships better, leading to better predictions of CP placements. FNN captured data characteristics better and produced superior results compared to K-means and random forest models.
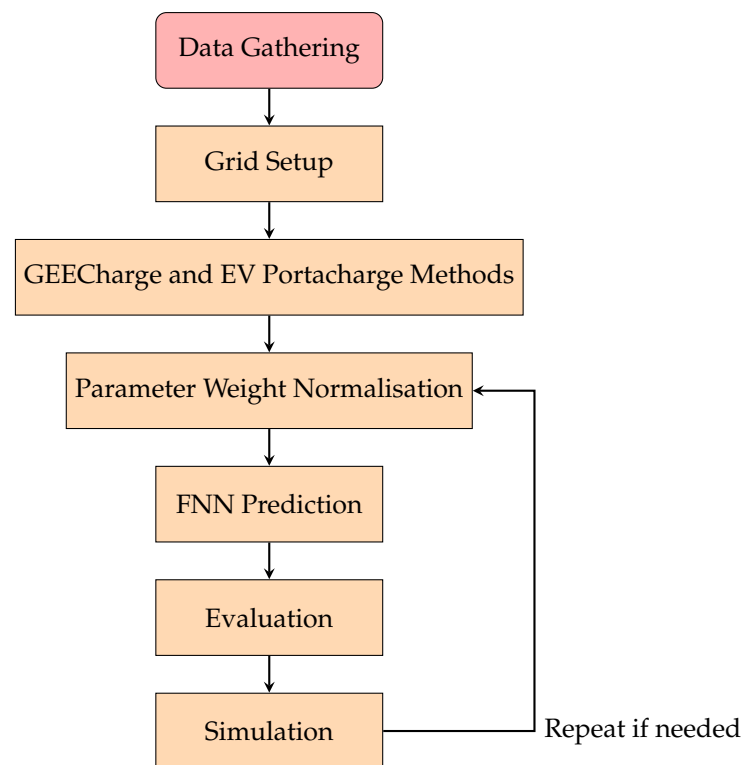
Figure 1. This flowchart outlines the key steps involved in our research methodology. Starting with data gathering, we proceeded to establish a grid setup. Subsequently, we employed the GEECharge and EV Portacharge methods to acquire relevant data. To ensure consistency and comparability, parameter weight normalisation was then applied. The normalised data were fed into a FNN for prediction, followed by a rigorous evaluation process. Based on the evaluation results, a simulation was conducted to assess the performance of the proposed approach. This iterative process, involving adjustments and repetitions as needed, leads to a refined and optimised methodology.

3.1. Gathering Traffic Data

We consider a 6 km × 10 km area in Dublin, which covers the central part of the city, as illustrated in Figure 2. Every hour, we gather information on how many vehicles are using each Dublin junction. As seen in Figure 3, we utilise these data to produce a heat map that illustrates traffic congestion. We make mapping more effective by splitting the area into 1 km × 1 km square cells [14]. Square grids are commonly used in urban planning studies, for example, reference [14]: Martí, P.; Jordán, J.; Palanca, J.; Julian, V. "Charging stations and mobility data generators for agent-based simulations. Neurocomputing 2022, 484, 196–210". There is a practical reason for this. In urban settings, road networks and land use are generally aligned to an orthogonal grid, for example, blocks and streets. Square grids match well with these alignments, allowing for better adaptation to the physical infrastructure of cities. We adopt a square grid to facilitate easy comparison with related methods in the literature. The grid is denoted as $\mathcal{G}$, and r and c represent rows and columns, respectively. We define $\mathcal{G}$ as a set representing the grid of cells ranging from $(1,1)$ to $(6,10)$. We express this as follows:

$$\mathcal{G} = \{(r,c) \mid r \in \{1,2,\ldots,6\}, c \in \{1,2,\ldots,10\}\}. \tag{7}$$

Figure 2. Dublin area divided into 1 km² cells. A cell of 1 km² size is suitable since it ensures that all areas are comprehensively covered and CPs are efficiently distributed. This guarantees that CPs are ideally suited within suitable driving distance.

We determine the most used roads using Google Earth and join adjacent sites using blues lines, as seen in Figure 4. We create a file containing the location of each intersection controlled by the Sydney Coordinated Adaptive Traffic System (SCATS) associated with values $(0, 1)$. In the selected grid in Dublin, we retrieve traffic data with unique IDs that show the time, region in the city, site, and volume of cars. We calculate the daily average number of cars $\mu_{\hat{c}_i}$ for each unique ID as follows:

$$\mu_{\hat{c}_i} = \frac{S_i}{30}, \tag{8}$$

where 30 represents days in a month. Here, S_i is the total sum of cars for a specific ID I in the traffic data file $I_{\hat{t}}(j)$, provided that it matches the location ID file $I_{\hat{l}}(i)$. The sum S_i is calculated as follows:

$$S_i = \sum_{j \in J} n_{\hat{c}}(j) \delta(I_{\hat{t}}(j), I_{\hat{l}}(i)), \tag{9}$$

where the function $n_{\hat{c}}(j)$ returns the traffic count, and $\delta(I_{\hat{t}}(j), I_{\hat{l}}(i))$ is a matching function that ensures the traffic data ID $I_{\hat{t}}(j)$ matches the location data ID $I_{\hat{l}}(i)$. The δ function returns 1 if the IDs are equal and 0 otherwise. To synchronise the traffic data and location data, we use i and j as simple index variables. These indices increment when the conditions below are met, ensuring that the records align correctly:

$$i = \begin{cases} i + 1 & \text{if } I_{\hat{t}}(j) < I_{\hat{l}}(i), \\ i & \text{otherwise} \end{cases}, \tag{10}$$

and

$$j = \begin{cases} j + 1 & \text{if } I_{\hat{t}}(j) > I_{\hat{l}}(i), \\ j & \text{otherwise} \end{cases}. \tag{11}$$

We use i and j purely as indexing variables to match the data from two sources, helping to iterate through the dataset.
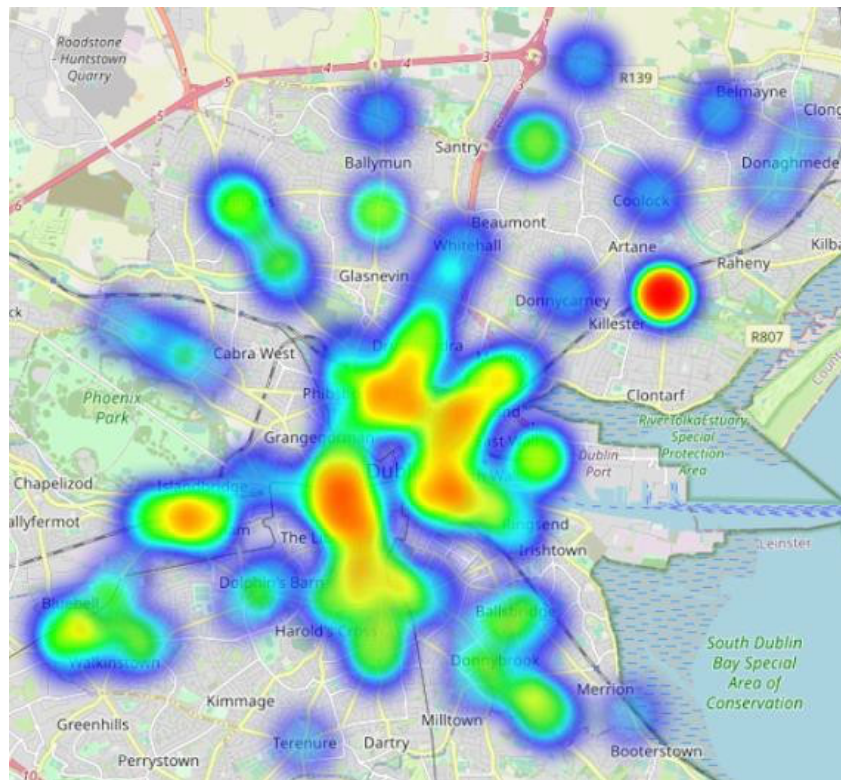
Figure 3. Heat map showing traffic and location intersections. The heat map shows the congested junctions in different areas of Dublin. The gradient illustrates the level of congestion at junctions, going from blue (indicating no congestion) to red (indicating total congestion).

Figure 4. The figure displays the busiest roads in June 2021, represented in a grid on a map of Dublin. Similar square cells of 1×1 km have been created from the grid. The blue lines show the frequently used highways. The black font represents grid cell coordinates and indices. The columns are represented by c and the rows by r. The dots indicate that c is increasing from 1 to 10 and r is increasing from 1 to 6.

3.2. Rotated Grid of the Dublin Area

We denote a point in the original grid as (x, y), representing its original coordinates before rotation, and the rotated point as (x', y'), representing its new coordinates after rotation. To perform the rotation, we rotate the point around the centre (cx, cy) by an angle θ [90,91]. We transform (x, y) to (x', y') as follows:

$$x' = (x - cx)\cos\left(\theta\frac{\pi}{180}\right) - (y - cy)\sin\left(\theta\frac{\pi}{180}\right) + cx, \tag{12}$$

$$y' = (x - cx)\sin\left(\theta\frac{\pi}{180}\right) + (y - cy)\cos\left(\theta\frac{\pi}{180}\right) + cy. \tag{13}$$

We represent the rotated position of the point $p = (x, y)$ as $p' = (x', y')$, where we apply the rotation matrix $\boldsymbol{R}(\theta)$ to p, with the matrix adjusted to account for the centre (cx, cy). We define the rotation matrix as follows:

$$\boldsymbol{R}(\theta) = \begin{bmatrix} \cos\left(\theta\frac{\pi}{180}\right) & -\sin\left(\theta\frac{\pi}{180}\right) \\ \sin\left(\theta\frac{\pi}{180}\right) & \cos\left(\theta\frac{\pi}{180}\right) \end{bmatrix}. \tag{14}$$
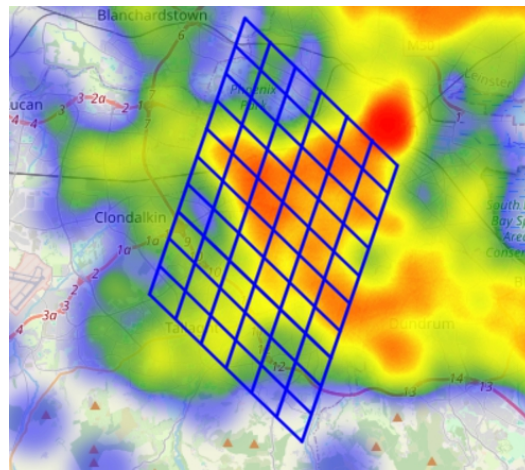
Figure 5. Grid rotated at an angle of 30°. The visualisation represents a heat map with a rotated grid on the Dublin map. Blue indicates low population density, and red indicates high population density. When the grid is rotated, it reduces the regions with high population density being covered.
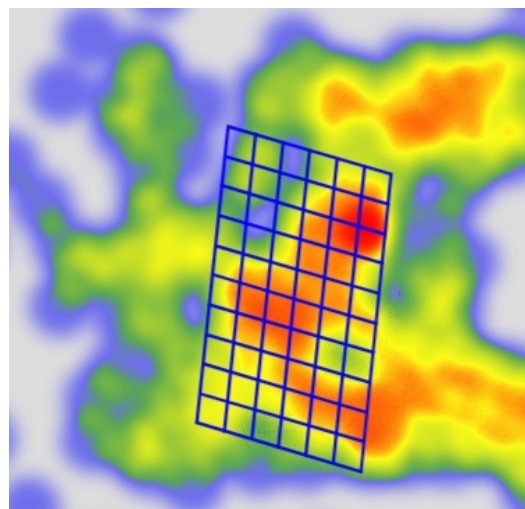
Figure 6. Grid rotated at an angle of −350°. The grid covers more cells compared to other angle rotations. This leads to a 5.7% increase in the total number of CPs in the grid as the number of CPs increases from 7552 in the original grid to 7982 in the rotated grid, as more cells with high population density are covered.

Grid rotation influences CP distribution as shown in Figure 5 and Figure 6.

3.3. Reducing the Size of Dublin's Grid Cells

We decide to reduce the size of the cells by half, from 1 km^2 to 500 m^2, to observe the effect on the distribution of CPs in Dublin. This reduction in cell size increases the number of cells from 60 to 120 and the grid size from 6 km by 10 km to 10 km by 12 km. We now have greater granularity and flexibility in allocating CPs. This allows us to adjust the weights for each smaller cell more precisely.
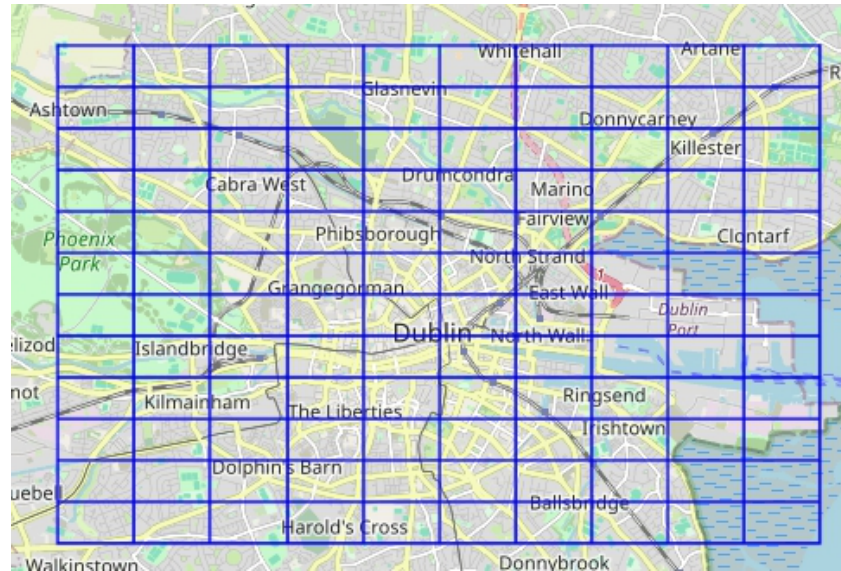
Figure 7. Reduced grid cells of each size, 500 m. We find that in smaller cells, CPs are more close to each other, and thus, $d(i, j)$ between v_i and CP z_j is reduced. For instance, we evaluate the distribution of 81 CPs in $\mathcal{G}_{11}$ when the size is 1 km^2 and again when the size is 500 m^2. Results show that the mean distance reduces from 37.28 to 22.67.

Reducing the grid cell size, as shown in Figure 7, decreases the average distance from 37.28 m to 22.67 m, bringing CPs closer to EVs. This proximity reduces range anxiety, as EV drivers can access charging stations more easily and quickly when needed.

3.4. GEECharge and EV Portacharge Methods

By considering the population density and POIs, we evaluate two approaches to distribute CPs in Dublin. The first solution s_1 proposed is, namely, the EV Portacharge. Scores are assigned by the EV Portacharge technique according to POIs and population density factors. The second technique, GEECharge, adds frequently used roads as a factor. We make use of the population density of 2021, where we represent the lowest density as 1 and the highest density as 6. We selected various POIs, such as university campuses, supermarkets, hospitals, cinemas, and tourist places, to represent the POIs in Dublin. We assigned scores to cells based on the number of POIs in a cell. In this case, 20 represents the maximum number of POIs in a cell. The justification for this is outlined as follows. We consider the population density to follow a normal distribution. This is consistent with the approach in [92]. According to the empirical rule for normal distribution, 99.7% of data points fall within three standard deviations above or below the mean. This translates to dividing the range into six equal intervals, where each interval corresponds to one standard deviation. By setting six intervals from lowest to highest, we represent distinct portions of the population density range.

Population density cells are represented as $d(r, c) = d_1, d_2, d_3, \ldots, d_{60}$, where $d_1 = \{x_1, y_1\}, d_2 = \{x_2, y_2\}, \ldots, d_{60} = \{x_{60}, y_{60}\}$ indicate the population density scores.

The grid forms a 6×10 matrix, so d_{60} corresponds to the population density score for the cell located at the 6th row and 10th column of the grid.

- Define $d(r,c)$ as the population density in cell (r,c), where r denotes the row number and c represents the column number, as shown in Figure 4.
- Define $p(r,c)$ as the count of points of interest (POIs) within cell (r,c).
- Let $s_1(r,c)$ represent the score assigned to cell (r,c) using the EV Portacharge method.
- Let $s_2(r,c)$ denote the score given to cell (r,c) according to the GEECharge method.

POIs are represented as $p(r,c) = p_1, p_2, p_3, \ldots, p_{60}$, where each $p_1(d_1), p_2(d_2), \ldots, p_{60}(d_{60})$ corresponds to the POI scores for each cell. The values are scaled by the weights w_d and w_p, with higher weights increasing the contribution of their respective values. The score for each cell, $s_1(r,c)$, as assigned by the EV Portacharge method, is computed as shown below:

$$s_1(r,c) = \frac{d(r,c)w_d + p(r,c)w_p}{\sum_{r=1}^{6} \sum_{c=1}^{10} d(r,c)w_d + p(r,c)w_p} 100. \tag{15}$$

Scores of POIs range from $0 \leq p \leq 20$, while population density scores fall within $1 \leq d \leq 6$. A weight of $w_d = 4$ is applied to the population density, amplifying its influence to be four times greater than that of the POI component, which has a weight of $w_p = 1$. The final computed value is expressed as a percentage of the total number of CPs.

3.5. GEECharge Method

We assess the most frequently used roads with a similar calculation approach. Let $u(t)$ represent the usage score for road t, where $u(t) = t_1, t_2, \ldots, t_{60}$, and w_t is the corresponding weight. The frequently used roads in the network are determined by the maximum traffic flow between vertices v_i and v_j, represented as $f(v_i, v_j)$, where $\forall \{v_i, v_j\} \in E$. The set of the most frequently used roads denoted as R is defined by the following:

$$R = \text{sort}(f(v_i, v_j) | \{v_i, v_j\} \in E), \tag{16}$$

and $R[1]$ corresponds to the first element of the sorted list of maximum traffic flows between all vertices in the network graph. The score assigned by the GEECharge method is $s_2(r,c)$ and is computed as follows:

$$s_2(r,c) = \frac{d(r,c)w_d + p(r,c)w_p + t(r,c)w_t}{\sum_{r=1}^{6} \sum_{c=1}^{10} d(r,c)w_d + p(r,c)w_p + t(r,c)w_t} \times 100. \tag{17}$$

Road usage scores range from $0 \leq u \leq 4$, with a weight of $w_t = 10$ applied. The GEECharge method places twice as much emphasis on road usage compared to the combined weights of w_p and w_d. We have developed an algorithm to generate CP coordinates based on a predefined grid and input data from a CSV file. The initial latitude and longitude are indicated as x_1 and y_1, respectively. The grid cells are mapped from coordinates (x_1, y_1) in the northwest to (x_6, y_{10}), as illustrated in Figure 4.

Let x_0 and y_0 represent the starting latitude and longitude. The size of each cell along the x axis and y axis is given by Δx and Δy, respectively. The area contains n_x cells in the x direction and n_y cells in the y direction. We use i and j as indices to label each cell, where i ranges from 0 to $n_x - 1$ in the x direction, and j ranges from 0 to $n_y - 1$ in the y direction. The boundary of the ith cell in the x direction is $x_i = x_0 + i\Delta x$, and the boundary for the next cell is $x_{i+1} = x_i + \Delta x$. In the y direction, the boundary of the jth cell is $y_j = y_0 + j\Delta y$, and the boundary for the next cell is $y_{j+1} = y_j + \Delta y$. To generate random coordinates within a cell, we use the function U. The random x-coordinate for a point in cell (i, j) is $x_{ij} = U(x_i, x_{i+1})$, and the random y-coordinate is $y_{ij} = U(y_j, y_{j+1})$. This ensures that the generated coordinates fall within the cell boundaries. The total number of charging points (CPs) in a cell is denoted by Q, and the function $Q_{CP}(i, j)$ returns the number of CPs for the cell at indices (i, j).
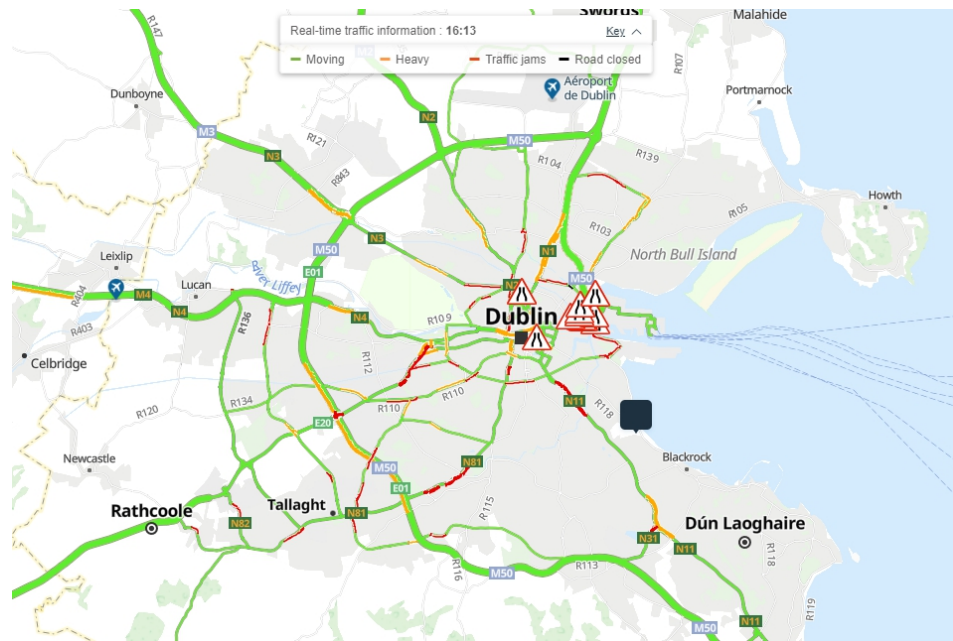
Figure 8. This graph shows traffic on Dublin roads at approximately 4 pm on a weekday. From the analysis we note that traffic is heavy at peak hours, that is in the morning and in the evening according to the authors of [93].

In Figure 8, the green sections show traffic is moving while the red sections show traffic congestion. The symbols indicate that some roads are narrowing ahead. On the timescale of parameters, we use 2022 electoral data for population density and represent them as P_{2022}. Population density in urban areas often follows periodic patterns due to daily, weekly, or seasonal cycles, such as daily variations due to commuting patterns, weather, or holidays. We present population density as follows:

$$P(t) = P_{2022}(1 + a_p \sin(\omega_p t + \phi_p)), \tag{18}$$

where amplitude a_p is population variation, ω_p is the frequency of population density variation, and ϕ_p is the phase shift.

It is tempting to classify POIs based on their attractiveness. POIs with low attractiveness could be excluded, and those with high attractiveness retained in order to prevent the overabundance of less attractive POIs from interfering with the final weighting of CPs allocation. We considered the number of POIs in cells instead of their attractiveness. By focusing on the number of POIs, we treat all areas as having the potential to influence charging demand. The rationale for this approach is that detailed data on the attractiveness of different POIs may not always be available. For the POIs, the number of people varies every single hour and depends on the location and type of POIs. Let $n(l, \tau)$ represent the number of people at location l at time τ. The baseline of the number of people at POI l is represented by $A(l)$. We develop a model to show the variation in the number of people at l, where we use the gym as an example and express it as follows:

$$n(l, \tau) = A(l)(1 + a \cos(\omega \tau + \phi)) + \epsilon(l, \tau), \tag{19}$$

where the amplitude of variation is a, and ω shows the frequency of variation. The phase shift in the model is ϕ, and $\epsilon(l, \tau)$ accounts for stochastic variations. For example, gyms tend to have more people in the evening and early in the morning. We express the model to account for morning and evening peaks as follows:

$$n_g(l, \tau) = A_g(l)\left[1 + a_{g1}\cos\left(\frac{2\pi\tau}{24} + \phi_{g1}\right) + a_{g2}\cos\left(\frac{2\pi\tau}{24} + \phi_{g2}\right)\right] + \epsilon(l, \tau), \tag{20}$$

where a_{g1} and a_{g2} are the amplitudes of the morning and evening peak variations, respectively. The phase shifts to align with the morning and evening peaks are ϕ_{g1} and ϕ_{g2}, respectively. For the most used roads, traffic data vary every hour, with heavy traffic during peak hours. We model this as follows:

$$T(t, \tau) = A_t \left[1 + a_t \sin\left(\frac{2\pi(\tau - \tau_{\hat{p}1})}{24} + \phi_{t1} \right) + b_t \sin\left(\frac{2\pi(\tau - \tau_{\hat{p}2})}{24} + \phi_{t2} \right) \right] + \eta_t(\tau), \quad (21)$$

where A_t represents the baseline traffic flow on road t, the amplitudes of the traffic peaks are represented by a_t and b_t, and $\tau_{\hat{p}1}$ and $\tau_{\hat{p}2}$ are the peak traffic times. Traffic fluctuation is represented by $\eta_t(\tau)$. In $T(t, \tau)$, t represents the road, while in $n(l, \tau)$, τ represents the time.

3.5.1. Parameter Weight Normalisation

We sum the weights to 1 to have equity in their contribution to CP distribution in Dublin. We first set w_d to 1 and w_p to 0 and then decreased w_d slowly to 0 as w_p increased to 1. This ensures that their sum is 1 at every instance. We then use each set of weight combinations to determine the corresponding CPs and find the $d(i, j)$. We observe the changes in $d(i, j)$ and success rate. The total weight γ is the sum of w_d and w_p, where

$$\gamma = w_d + w_p. \quad (22)$$

We normalise weights as follows:

$$\hat{w}_d = \frac{w_d}{\gamma}, \quad (23)$$

$$\hat{w}_p = \frac{w_p}{\gamma}. \quad (24)$$

The most used roads normalised weight is denoted as $\hat{w}_t$. The sum of all weights is equal to one, where

$$\kappa + \hat{w}_t = 1. \quad (25)$$

Since the value of κ changes as the value of $\hat{w}_t$ varies, we say

$$\hat{w}_{d_i} = \hat{w}_d \kappa, \quad (26)$$

where $\hat{w}_{d_i}$ is the population density normalised weight of a specific cell indexed by i.

$$\hat{w}_{p_i} = \hat{w}_p \kappa, \quad (27)$$

where $\hat{w}_{p_i}$ is the point of interest normalised weight of a specific cell indexed by i.

$$\hat{w}_{d_i} + \hat{w}_{p_i} + \hat{w}_{t_i} = 1, \quad (28)$$

where $\hat{w}_{t_i}$ is the most used roads normalised weight of a specific cell. We calculate the MSE as follows:

$$\sigma = \frac{1}{N} \sum_{i=1}^{N} (y_i - \hat{y}_i)^2, \quad (29)$$

where N is the total number of points, and a single point is the distance between an EV location and a CP location. Notation y_i is the actual mean distance, and $\hat{y}_i$ is the expected mean distance.

3.6. Using Feedforward Neural Networks (FNNs)

We created a large dataset to distribute EV CPs across the grid using the weights w_d, w_p, and w_t. The w_d scores range from 1 to 6 and represent population density levels. The

weight, w_p, represents the number of POIs in a location. It ranges from 0 to 20. The weight, w_t, represents traffic on the most used roads. It has scores ranging from 0 to 4. Weight combinations for these parameters were generated using normalised weights ranging from 0 to 1. For each combination, we calculated the GEECharge score to allocate CPs across the grid. We saved the scores and the corresponding CPs in a CSV file for further processing. The total number of CPs per cell was determined by distributing them based on this score, ensuring that cells with higher w_d, more w_p, and greater w_t received a larger number of CPs. Each row in the dataset represented a unique combination of these weights, along with the corresponding grid cell location (row and column) and the number of CPs assigned. These combinations include scenarios shown in the equations below:

$$w_d = w_p = w_t, \tag{30}$$

$$w_d = w_p + w_t, \tag{31}$$

$$w_t = w_d + w_p, \tag{32}$$

$$w_t = k(w_d + w_p), \tag{33}$$

where $k = 2, 3, 4, 5, 6$. Population density w_d, being equal to w_p and w_t, serves as a baseline as we are giving equal importance to all parameters. This helps us understand how the parameters influence the distribution of CPs. Population density w_d, being equal to the sum of w_p and w_t, prioritises areas with high population density, as they are more likely to have a higher EV adoption rate. The most used roads w_t, being equal to the sum of w_d and w_p, shows the importance of high-traffic areas since placing CPs along a busy road can serve many EVs. Increasing w_t to be thrice to six times the sum of w_d and w_p is useful in areas with vast road networks. Experimenting with different combinations of weights helps us model the most effective strategies to meet EV user needs.
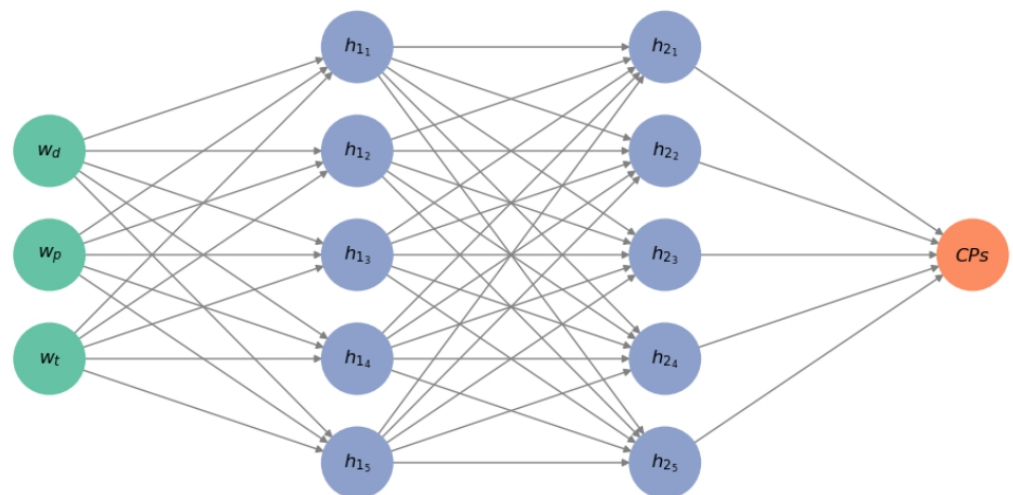
Figure 9. The graph shows a FNN where GEECharge parameters w_d, w_p, w_t are the inputs of the network, and the network predicts the number of CPs in a given cell. In the FNN, output CPs are generated after the inputs have been processed through hidden layers.

During experimentation, we compared the performance of our approach with K-means and random forest variants of the CP allocation algorithm in order to identify the most suitable approach for predicting CP locations. The results demonstrated that the FNN approach provided a more balanced weighting solution and better captured the characteristics of data. The rationale for this result is that K-means is typically used as a clustering algorithm, which is designed for grouping data into clusters based on similarity, for example, using the squared Euclidean distance as a measure of error, rather than for predictive modelling. In addition, we observed that random forests struggled to deliver the

same performance as FNNs. We decided to use FNNs as shown in Figure 9 as they provide a more balanced solution and capture non-linear relationships in the data. We use a FNN, TensorFlow, and Keras to predict the number of CPs for a specific cell. The input layer has three neurons corresponding to the features w_d, w_p, and w_t. The weights are input as a vector expressed as follows:

$$B = [w_d, w_p, w_t]. \tag{34}$$

There are five hidden layers of different numbers of neurons (256, 256, 128, 64, and 32) which learn the features of data. We extract features in the data while still managing the possible risks of under-fitting and over-fitting. Each hidden layer performs a linear transformation followed by an activation function, denoted as σ. Let L be the total number of hidden layers. Then, for the kth hidden layer, where $k = 1, 2, \ldots, L$,

$$h_k = \sigma(h_{k-1} W_k + b_k), \tag{35}$$

where the input layer is $h_0 = B$, $W_k \in \mathbb{R}^{n_{k-1} \times n_k}$ are the weights for the kth hidden layer, and $b_k \in \mathbb{R}^{n_k}$ are the biases for the kth hidden layer. Here, n_{k-1} and n_k are the number of neurons in the $(k-1)^{th}$ and k^{th} layers, respectively.

We standardise the parameter features and scale them to a mean of 0 and a standard deviation of 1, ensuring that the weights have equal contributions in CP distribution. We split the dataset into training and testing sets. We use the activation function σ for non-linearity. Dropout prevents over-fitting by randomly setting a fraction of input units to 0 during training. We express this as follows:

$$h'_k = d_p(h_k), \quad \text{for } k = 1, 2, 3, 4, 5, \tag{36}$$

where d_p is the dropout function. The output layer consists of a single neuron since it is a regression problem. We express this as follows:

$$CP = h'_5 W_6 + b_6, \tag{37}$$

where $W_6 \in \mathbb{R}^{32 \times 1}$ are the weights connecting the 5th hidden layer to the output layer, and $b_6 \in \mathbb{R}^1$ is the bias term for the output layer. We compile the model using the Adam optimiser and the MSE loss function, where the Adam optimiser helps to minimise the loss function during training. The data are trained using 30 epochs, and validation data are used to monitor the performance of the model. The choice of 30 epochs is based on empirical validation and also to balance under-fitting and over-fitting. We use the trained model to make predictions on the data to find the best parameter weight combination. The index of the combination with the least MSE is expressed as follows:

$$\hat{\sigma} = \frac{1}{N} \sum_{i=1}^{N} (z_i - f(v_i, w))^2, \tag{38}$$

where N is the number of data points, and z_i is the actual CP for the ith data point. The predicted CPs are encapsulated in the function $f(v, w)$, which takes input features v and weights w and produces an output, which is the predicted CP. In finding the best combination of weights w^* that minimises $\hat{\sigma}$, we use the following:

$$w^* = \arg\min_w \hat{\sigma}. \tag{39}$$

We compute the best index that corresponds to the best weight combination as follows:

$$i^* = \arg\min_i (z_i - f(v_i, w))^2. \tag{40}$$

The CPs are distributed across each cell according to a uniform distribution. This method helps to reduce the chance of CPs overlapping or being concentrated in one area. While the distribution algorithm ensures that CPs are evenly spread across the grid, congestion may still occur if there is high demand for a particular CP. The research does not account for CP capacity, but future research could work on how each CP can handle multiple EVs at the same time.

3.7. CP Distribution Efficiency

We define the efficiency metric η as a function of mean distance $\bar{d}$ and success rate R. Efficiency is inversely related to the mean distance and directly related to the success rate, where

$$\eta(\bar{d}, R) = \frac{R}{\bar{d}}. \tag{41}$$

We use the brute force search for optimal weights iterating through all possible combinations of the parameter weights w_t, w_d, and w_p. We consider the combination that results in the highest efficiency to be optimal. We describe this as follows:

$$\max_{w_t, w_d, w_p} \eta(\bar{d}, R) \quad \text{subject to: } w_t, w_d, w_p \geq 0 \quad w_t + w_d + w_p = 1. \tag{42}$$

The mean distances $\bar{d}$ and R are functions of w_t, w_d, and w_p, where

$$\bar{d} = f_{\bar{d}}(w_t, w_d, w_p), \quad R = f_R(w_t, w_d, w_p). \tag{43}$$

Functions $f_{\bar{d}}$ and f_R are derived from data showing how the weights influence $\bar{d}$ and R. Using these functions, we rewrite the efficiency η as follows:

$$\eta(w_t, w_d, w_p) = \frac{f_{\bar{d}}(w_t, w_d, w_p)}{f_R(w_t, w_d, w_p)}. \tag{44}$$

We optimize $\eta(\bar{d}, R)$ by finding the set of weights that results in the smallest value of η. This optimisation is formulated as follows:

$$\min_{w_t, w_d, w_p} \left(\frac{f_{\bar{d}}(w_t, w_d, w_p)}{f_R(w_t, w_d, w_p)} \right) \quad \text{, subject to: } w_t + w_d + w_p = 1, \text{ and } w_t, w_d, w_p \geq 0. \tag{45}$$

The optimal weights (w_t^*, w_d^*, w_p^*) solve the optimisation problem. We define the maximum efficiency $\eta_{\max}$ as follows:

$$\eta_{\max} = \eta(w_t^*, w_d^*, w_p^*) = \min_{w_t, w_d, w_p} \eta(w_t, w_d, w_p). \tag{46}$$

We use the conditional expectation to see how the expected efficiency $\eta[Y|w_t]$ changes with different values of w_t given a model $f(w_t, w_d, w_p)$. This is expressed as follows:

$$\eta[Q|w_t] = \eta[f(w_t, w_d, w_p)|w_t]. \tag{47}$$

The total number of CPs is represented by Q. The pseudo-code for CP prediction using FNN is shown in Algorithm 1.

Algorithm 1 This algorithm outlines the prediction of an optimal number of CPs in a cell using a FNN. The FNN takes in weights and CPs from GEECharge and predicts the optimal number of CPs in a cell and the corresponding weights that minimise the prediction error.

Require: w_d, w_p, w_t
1:   $CPs \leftarrow []$
2:   $scores \leftarrow [][]$
3:   **Dataset Generation:**
4:   **for** each cell (r, c) **do**
5:      Generate w_d, w_p, w_t combinations: $w_d = w_p = w_t$, $w_d = w_p + w_t$, $w_t = k(w_d + w_p)$, where $k = 2, 3, 4, 5, 6$
6:      Compute GEECharge score $s_2(r, c)$
7:      Store $s_2(r, c)$ in *scores*
8:   **end for**
9:   **FNN:**
10:   Input: 3 neurons $[w_d, w_p, w_t]$
11:   Hidden layers: $[256, 256, 128, 64, 32]$
12:   Output: 1 neuron (CP prediction)
13:   Activation: ReLU
14:   Standardise features
15:   **FNN Training:**
16:   Forward propagation, Adam optimiser, MSE loss
17:   Train for 30 epochs
18:   **CP Prediction:**
19:   **for** each cell (r, c) **do**
20:      Predict CPs with FNN
21:      Compute MSE: $\hat{\sigma} = \frac{1}{N} \sum_{i=1}^{N} (z_i - f(v_i, w))^2$
22:   **end for**
23:   Find optimal w^* minimizing $\hat{\sigma}$
24:   Ensure uniform CP distribution **return** Predicted *CPs*

---

4. Evaluating GEECharge

We implement a discrete event simulation (DES) approach to simulate trips across the Dublin Road network to evaluate the GEECharge and EV Portacharge methods. Let $G_z = (C, E)$ represent a subgraph of G containing the vertices and edges associated with the CPs and their connections. An EV situated at vertex v_i in G can reach the closest charging point z_j in G_z by calculating the shortest path between v_i and z_j in G_z using Dijkstra's algorithm. The set of all CPs in the subgraph G_z is denoted by C, represented as $C = \{z_1, z_2, z_3, \ldots, z_q, \ldots, z_Q\}$, where z_q refers to the qth CP, and Q is the total number of CPs. The nearest CP z_j to the vertex v_i is determined by minimising the distance metric $d(i, j)$ between v_i and z_j, expressed as follows:

$$z^\star \leftarrow \arg\min\{d(i, j) \mid z_j \in C\}. \tag{48}$$

When an EV's battery is depleted, the Euclidean distance between its current position and the nearest CP is computed. This distance is defined as the shortest path between the EV's location $l(v_i)$ and the location of the CP $l(z_j)$. We simulate a chosen number of cars and provide trip statistics.

In the road traffic simulation, we model EV interaction with the available CPs to evaluate the efficacy of CP placement. For each EV i, where $i \in \{1, \ldots, \hat{N}\}$, we select a starting node $a_i^{(s)}$ from a set of all nodes N. The total number of cars is denoted by $\hat{N}$. We simulate the trip of each EV i by repeatedly selecting an end node $a_i^{(e)}$ randomly from N until the accumulated travel distance d_i satisfies $d_i \geq$ range. We compute distance d_i as follows:

$$d_i = \sum_{k=1}^{m} d(a_{i,k}^{(s)}, a_{i,k}^{(e)}), \tag{49}$$

where m is the number of segments travelled by car i, and d denotes the shortest path distance function. The coordinates $(x_{a^{(e)}}, y_{a^{(e)}})$ of the final node $a_i^{(e)}$ are used to calculate the nearest CP by the following:

$$d(i,j) = \min_{j \in CP} \{ E(x_{a^{(e)}}, y_{a^{(e)}}, x_j, y_j) \}, \tag{50}$$

where E represents the Euclidean distance calculation, and x_j, y_j are the coordinates of CP j. The Euclidean distance in m between a CP and the arrival node is determined using the haversine formula. The magnitude of the vector formed by the difference between $a_i^{(s)}$ and $a_i^{(e)}$ is calculated as follows:

$$\left\| l(a_i^{(s)}) - l(z_j) \right\| = ||x_i - x_j| - |y_i - y_j||, \tag{51}$$

where $l(a_i^{(s)}) = [x_i, y_i]$ and $l(z_j) = [x_j, y_j]$. This can also be expressed using absolute values as follows:

$$||x_i - x_j| - |y_i - y_j||, \tag{52}$$

where (x_i, y_i) and (x_j, y_j) are the coordinates of the vertices $a_i^{(s)}$ and CP z_j, respectively. The distance $d(i,j)$ is computed by defining $\varphi = x_j - x_i$ and $\lambda = y_j - y_i$. Since the grid size is 6 by 10, the coordinates x_i range from 1 to 6, and y_i range from 1 to 10. The haversine formula for calculating the distance between two points on the Earth's surface is as follows:

$$d(i,j) = 2R \arcsin \sqrt{\sin^2 \frac{\varphi}{2} + \cos \varphi_1 \cos \varphi_2 \sin^2 \frac{\lambda}{2}}. \tag{53}$$

Here, the Earth's radius is approximately $R \approx 6371$ km, and variables φ and λ represent the differences in the coordinates x_i and x_j, and y_i and y_j, respectively, as shown in Equation (53). The equation above expresses $d(i,j)$ as the Euclidean distance between the two points. We use GEECharge to maximise the efficacy of CP placement by combining w_d, w_p, and w_p. FNNs can learn these relationships better, leading to better predictions of CP placements. We use parameter weight normalisation to ensure that there is equity in weight contribution in CP distribution.

5. GEECharge Weight Analysis

We provide a summary of the results, which we then utilise to organise the experiment descriptions. We show the following:

1. Points of interest (POIs), population density, and most used roads normalised optimal weights are $w_d = 0.1339$, $w_p = 0.4018$, $w_t = 0.4444$, respectively.
2. Optimal parameter weights give 109 CPs in a 1 km^2 area.
3. Resizing the grid to 10 by 6 and rotating it at an angle of $-350°$ increases the total number of CPs by 5.7%, enhancing coverage.
4. Reducing the grid by half to smaller cells, CPs are closer to each other, and thus, $d(i,j)$ between v_i and CP z_j is reduced. For instance, we evaluate the distribution of 81 CPs in $\mathcal{G}_{11}$ when the size is 1 km^2 and again when the size is 500 m^2. Results show that the mean distance reduces from 37.28 m to 22.67 m.
5. FNN trains the data and predicts the best weight combinations.
6. We determine the CP distribution efficiency in Dublin.
7. We normalise all the weight for equity in CP distribution.

We simulate EVs finding the nearest CPs from their current location within Dublin, where we select cell $(1,1) \in \mathcal{G}$ as the region of simulation. We represent cell $(1,1) \in \mathcal{G}$ as $\mathcal{G}_{11}$. Using real-world coordinates, we generate CP positions in the cells as shown in Table 5. To determine the most efficient route, we use the Haversine formula. We first select 100 EVs for simulation and calculate the distance between the EVs $l(v_i)$ and CPs $l(z_j)$. Once

the distances are established, we implement Dijkstra's algorithm to find the shortest path for an EV positioned at v_i in G to reach the closest CP z_j in G_z by determining the shortest path between v_i and z_j. We consider a trip as successful when an EV reaches a CP z_j that is within 100 m from its current location v_i.

Mean distance ($\bar{d}$):

$$\hat{d} = \frac{\sum d(i,j)}{\hat{N}}, \tag{54}$$

where $\hat{d}$ is the mean distance, $d(i,j)$ is the distance from the v_i and z_j in G_z, and $\hat{N}$ is the total number of EVs in the simulation.

Success rate (SR):

$$SR = \frac{\hat{C}_s}{\hat{N}} \times 100\%, \tag{55}$$

where SR is the success rate, $\hat{C}_s$ is the number of successful charges (that is, the EVs that find a CP within 100 m), and $\hat{N}$ is the total number of EVs in the simulation.

Table 5. The table shows the EV location and nearest CP. We show the latitude and longitude of the EV, indicating its exact geographical position, along with the distance to the nearest CP measured in m.

EV ID	Latitude (EV Location)	Longitude (EV Location)	Distance to Nearest CP (m)
1	53.38109	−6.32120	42.48
2	53.37488	−6.33384	39.12
3	53.38100	−6.32478	42.28
4	53.38123	−6.33291	90.00
5	53.37413	−6.32626	78.60
6	53.37869	−6.32303	91.32
7	53.37539	−6.33203	77.22
8	53.38239	−6.32838	16.44
9	53.37917	−6.32784	53.22
10	53.37616	−6.32471	8.76
11	53.37365	−6.33342	101.37
12	53.37938	−6.32977	119.48
13	53.37486	−6.33115	21.45
14	53.38147	−6.32812	64.95
15	53.37919	−6.33069	64.39
16	53.38088	−6.32093	23.12

We show the start points and the end points of trips in the EV simulation. The green dot in Figure 10 represents $l(v_i)$, and the red dot represents $l(z_j)$.
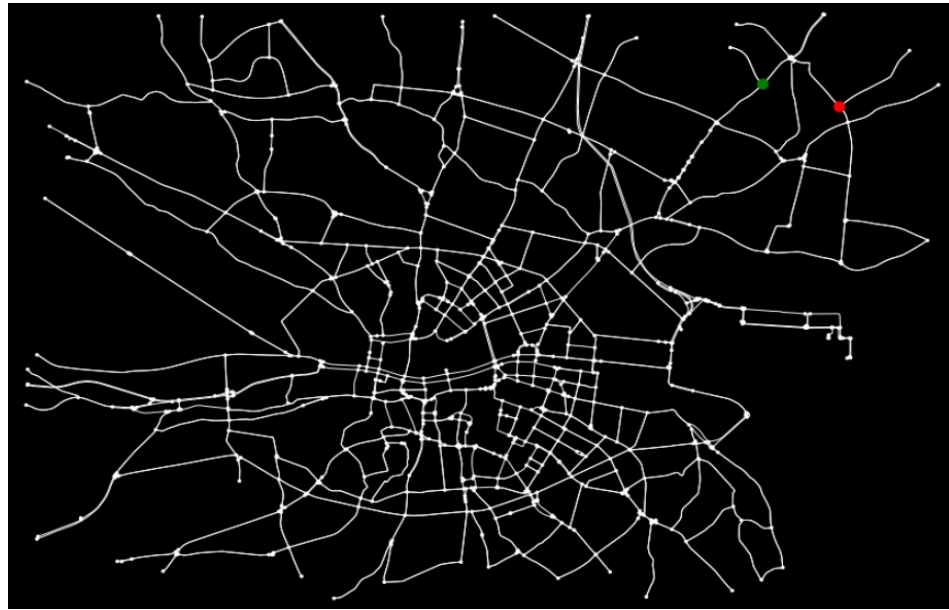
Figure 10. This graph shows the trip's start and end points for a sample EV. The start point is shown in green while the arrival point is shown in red.

In the first finding, we normalise parameter weights by summing the three weights and identifying the best combination. We combine w_d and w_p, where w_d varies from 1 to 0, and w_p varies from 0 to 1. The weights w_d and w_p are paired such that w_d decreases from 1 to 0 in increments of 0.1, while w_p increases from 0 to 1 in increments of 0.1. The weight pairs (w_d, w_p) range from $(1,0)$ to $(0,1)$ through $(0.9, 0.1), \dots, (0.1, 0.9)$. We analyse how the variation of w_d and w_p influences the distribution of CPs when normalised. We calculate the corresponding CPs for each pair and perform the EV simulation. We simulate the distance from the current EV location to the CP location and term it a success if the distance is less than 100 m from the EV location. We select $\mathcal{G}_{11}$ in the grid to perform simulation, and the results are below.

Table 6. The table shows the results for $\mathcal{G}_{11}$ when 57 EVs were used in the simulation. The number of CPs decreases as the values of w_d increase. The results show that as the number of CPs decreases, the mean distance increases as CPs are getting farther from the EVs. This reduces the success rate.

w_d	w_p	Number of CPs	Mean Dist (m)	Success (%)
1.0	0.0	81	60.05	89.47
0.9	0.1	60	71.78	75.44
0.8	0.2	50	83.75	63.16
0.7	0.3	44	94.06	52.63
0.6	0.4	39	92.74	54.39
0.5	0.5	36	95.61	50.88
0.4	0.6	34	94.98	54.39
0.3	0.7	32	101.59	49.12
0.2	0.8	31	105.49	45.61
0.1	0.9	29	109.42	42.11
0.0	1.0	28	115.01	40.35

The results in Table 6 show how w_d and w_p influence CP distribution. As w_d decreases, the number of CPs decreases, thus increasing the mean distance as CPs are few, thus being

far from the EVs. This also reduces the success rate. We now perform a second simulation using 100 EVs, and the results are shown in Table 7.

Table 7. The table shows the results for $\mathcal{G}_{11}$ when 100 EVs were used in the simulation. The number of CPs decreases as the values of w_d increase.

w_d	w_p	Number of CPs	Mean distance (m)	Success (%)
1.0	0.0	81	60.78	90.00
0.9	0.1	60	68.92	81.00
0.8	0.2	50	79.74	70.00
0.7	0.3	44	90.62	61.00
0.6	0.4	39	93.20	57.00
0.5	0.5	36	95.90	54.00
0.4	0.6	34	96.70	54.00
0.3	0.7	32	103.20	50.00
0.2	0.8	31	108.75	46.00
0.1	0.9	29	114.84	40.00
0.0	1.0	28	120.22	38.00

We see that the success rate is decreasing as the mean distance is increasing. This is due to the reducing trend of CPs. We visualise how the cell scores are impacted by weight changes and show the results in Figure 11.
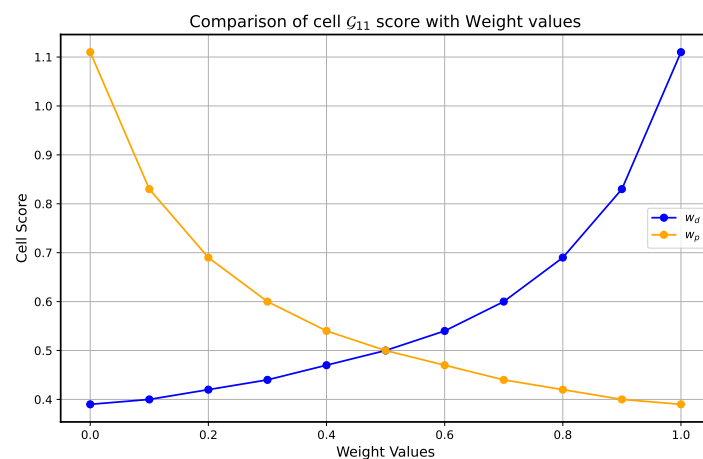
Figure 11. The graph shows that the cell scores vary as w_d and w_p vary. An increase in w_p leads to a subsequent increase in the $\mathcal{G}_{11}$ scores. Trends in the results show that balance between the two parameters is crucial in CP distribution.

We extract mean distances and w_p values and use a second degree polynomial to predict the expected mean distances from the current EV location to the CPs.

$$\hat{y}_i = aw_p^2 + bw_p + \hat{c}. \tag{56}$$

We obtain coefficients of the polynomial equation that best fit the mean distances corresponding to different w_p values. We now construct an equation to predict expected mean distances from the current EV location to the CP location, and it is expressed as follows:

$$\hat{d} = aw_p^2 + bw_p + \hat{c}. \tag{57}$$

The MSE for each w_p value is calculated by comparing the mean distances obtained from the parabolic fit with the actual mean distances. The results in Figure 12 can help policy makers in infrastructure resource allocation, as CPs are placed in areas they are most needed.
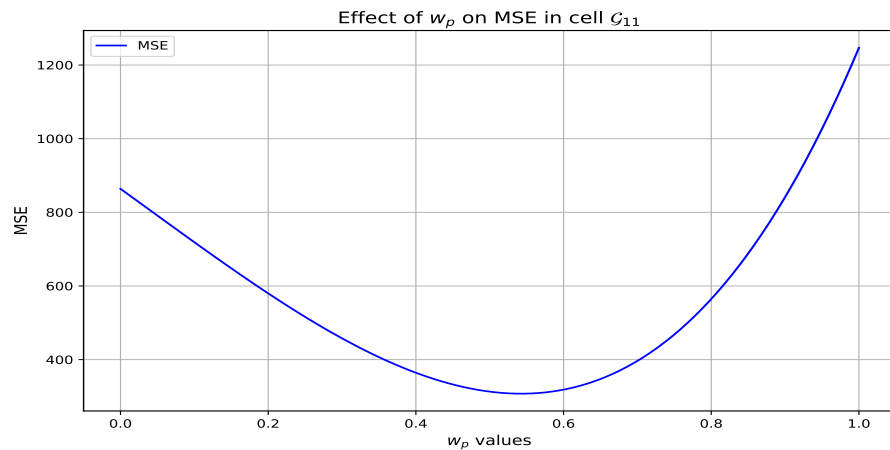
Figure 12. The graph shows the relationship between MSE and w_p. The MSE decreases as the weight increases up to approximately 0.545, then begins to increase. The value 0.545 is the optimal value as it gives the lowest MSE of 307.55. The results show that beyond 0.545, POIs' contribution becomes less effective due to overemphasis, highlighting the importance of weight balancing.

The results in Figure 13 show the importance of w_d in CP placement. With an optimal weight of 0.545, city planners can adopt a more strategic approach to infrastructure development. We add the weights of w_d and w_p, normalise them, and now vary w_t from 1 to 0, thus generating a range of weight combinations. We determine the percentage of CPs that are within 100 m of the EV's current location and compute the measure of success using the following equation:

$$\frac{1}{|C|} \sum_{z \in C} I(||l(v_i) - (z_j)|| < 100), \tag{58}$$

where $I(||l(v_i) - (z_j)|| < 100)$, is an indicator function that is equal to 1 if the distance between the EV's current location v_i and CP z_j is less than 100 m and equal to 0 otherwise. Before stopping, an EV can drive 1 km at a low speed to reach a CP. The simulation assumed approximately 100 cars passed through an intersection per hour, and most EVs had a range of approximately 400 km. While some EVs, like Tesla's Model S Long Range, offer a higher range of about 637 km, 400 km is typical for most EVs [94].

Table 7 shows different EV simulation results for an EV accessing a CP. Each row of the table corresponds to a distinct scenario with varying weight combinations of w_d and w_p, summing 1. The number of CPs column shows the total number of CPs resulting from each set of w_d and w_p weights. The mean distance is the average distance an EV must travel to reach the nearest CP. The success rate represents EVs that reach a CP that is within 100 m. A higher w_d reduces the mean distance and success rate if few CPs are placed.
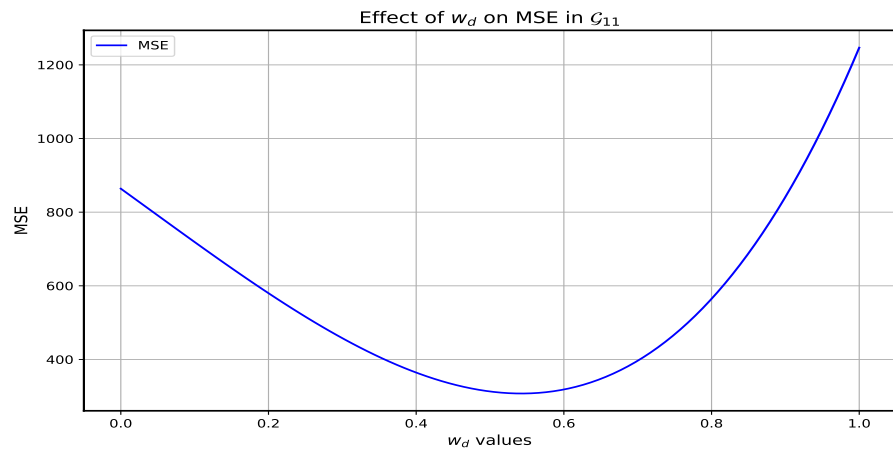
Figure 13. The graph shows the relationship between MSE and w_d. The MSE decreases as the weight increases up to approximately 0.545, then begins to increase. The value 0.545 is the optimal value as it gives the lowest MSE of 307.55. The results suggest that w_d is a significant factor in CP distribution and overemphasis on a single factor may affect CP distribution.

In Table 8, as the w_t increases, the number of CPs decreases to 0. When CPs are 0 in a cell, it means that an EV cannot access charge in that specific cell; thus, the distance is ∞.

Table 8. The table shows EV simulation in $\mathcal{G}_{11}$, using the three parameter weights. The results show that an increase in w_t leads to a decrease in the number of CPs in the cell. The decrease in CPs leads to a decrease in success rate due to an increase in the mean distance.

w_t	w_d	w_p	Number of CPs	Mean Distance (m)	Success Rate (%)
0.00	0.20	0.80	31	108.75	46.0
0.11	0.18	0.71	30	111.76	44.0
0.22	0.16	0.62	29	114.84	40.0
0.33	0.13	0.53	28	120.22	38.0
0.44	0.11	0.44	27	120.35	38.0
0.56	0.09	0.36	25	138.8	33.0
0.67	0.07	0.27	23	142.29	32.0
0.78	0.04	0.18	19	146.56	28.0
0.89	0.02	0.09	13	170.93	22.0
1.00	0.00	0.00	0	∞	0.0

Cell score varies on different weight values as shown in Figure 14. We calculate the MSE of the actual mean distance and the predicted mean distance and plot a graph of MSE against w_t, showing how an increase in w_t affects MSE. Figure 15 shows the results. As shown in Figure 16 we find that the optimal weights for parameters w_t, w_d, and w_p are 0.56, 0.09, and 0.36, respectively, with an MSE of approximately 379.41 and 382.50.
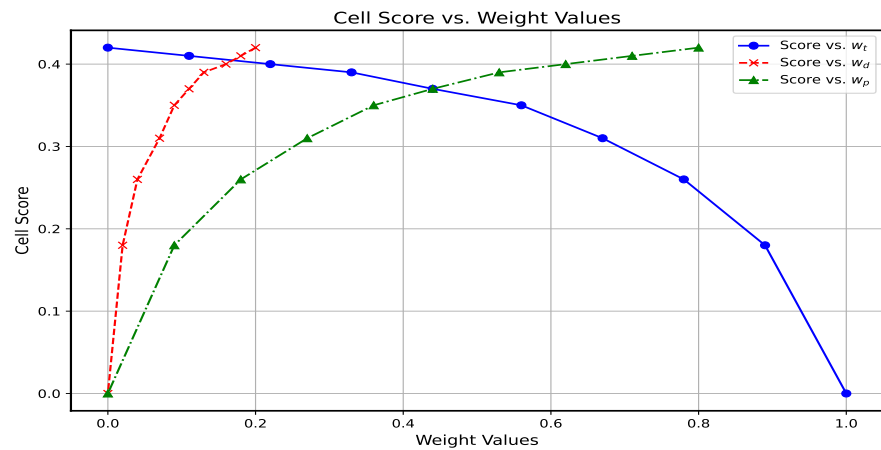
Figure 14. The graph shows the relationship between $\mathcal{G}_{11}$ scores and the three weights. The results show that the cell score increases as the w_d increases up to a certain point at which the curve begins to flatten. This implies that the impact of w_d on the score beyond that point diminishes. The cell score also increases with the increase in w_p. The cell score decreases as w_t increases. At first, the decrease is slow, but after approximately 0.6, there is a sharp decrease in the cell score. We see that w_t has a negative correlation beyond a certain point, suggesting that overemphasis on road usage may lead to sub optimal CP distribution.
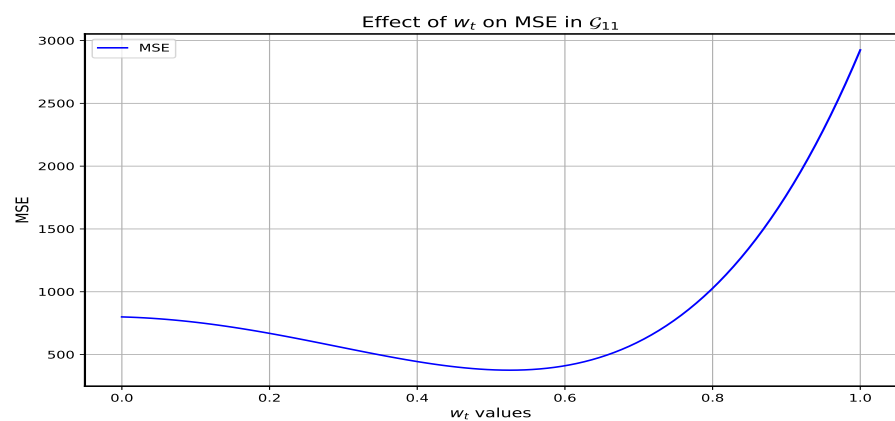
Figure 15. The graph shows the relationship between MSE and w_t. The MSE slightly decreases as the weight increases from 0.0 until it reaches approximately 0.525. The results show that 0.525 is the optimal w_t as it corresponds to the minimum MSE value of approximately 375.40. Beyond 0.525, we have a sharp increase in MSE. The results suggest that w_t significantly impacts MSE and that road score should be balanced to avoid being overly dominant.
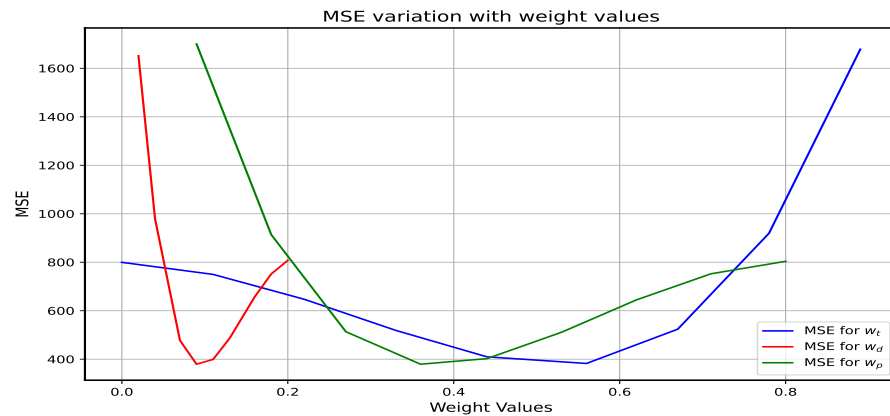
Figure 16. The graph shows the relationship between MSE and varying parameter weights. MSE slowly decreases as w_t increases from 0.0 to approximately 0.560 and then starts to sharply increase. MSE decreases as w_d increases to approximately 0.09 and then starts to increase. This suggests that a small value of w_d is sufficient to minimise the MSE error. The MSE decreases as w_p increases, reaching its minimum at approximately 0.360 with an MSE of 379.44. After this point, the MSE begins to increase slowly. The results show the need for balanced weighting of all parameters.

The FNN model predicts the optimal weights for population density, points of interest (POIs), and most used roads optimal weights as $w_d = 0.1339, w_p = 0.4018, w_t = 0.4444$ and the corresponding CPs as 109. To evaluate the effectiveness of our proposed FNN approach, we conducted comparative experiments with K-means and random forest algorithms. The results demonstrated that FNN consistently outperformed these methods in terms of accurately predicting CP locations and capturing the complex non-linear relationships within the data. The K-means algorithm provided a weight combination of $w_d = 0.1472$, $w_p = 0.7362$, and $w_t = 0.1111$ for the data set. The resulting CP allocation corresponded to 30 CPs being deployed. In this case, the weight w_p was more dominant over the other weights. The random forest approach yielded the weights $w_d = 0.2202, w_p = 0.6606$, and $w_t = 0.1111$. These weights resulted in 122 CPs being chosen. Similar to K-means, the weight w_p was more dominant compared to the other weights. The FNN results, however, showed a more balanced weight distribution across the three parameters than the K-means and random forest models.

We resize the grid to 10 rows and 6 columns and rotate at various angles to get the best position to place the grid. We find that $-350°$ increases the total number of CPs by 5.7% , enhancing coverage. This is because the total number of CPs increases from 7552 in the original grid to 7982 in the rotated grid as more cells with high population density are covered. For instance, cells $(6, 10)$ in the grid move from a position where we had no population density to a new position with a very high population density. This generally increases the number of CPs in the region. A 5.7% increase in CPs enhances the EV experience for drivers by improving accessibility and reducing wait times. This reduces range anxiety and boosts confidence in EV usage. For urban planners, this increase provides valuable data for strategically placing CPs, supporting policy initiatives, and integrating EV infrastructure into broader mobility strategies. This aligns with sustainability goals by promoting the adoption of EVs, reducing greenhouse gas emissions. Reduced number of CPs as shown in Table 9 could increase range anxiety and affect sustainability efforts.

Table 9. In $\mathcal{G}_{21}$, we use 290 EVs in the simulation. The results show that an increase in w_t leads to a decrease in the number of CPs in the cell. The decrease in CPs leads to a decrease in the success rate due to an increase in the mean distance. The mean distance increases from 79.74 m to 143.13 m. When w_t is set to 1, the total CPs is 0, and the EV mean distance becomes ∞.

w_t	w_d	w_p	Num Stations	Mean Dist (m)	Success Rate (%)
0.00	0.20	0.80	51	79.74	70.34
0.11	0.18	0.71	50	81.00	69.31
0.22	0.16	0.62	49	83.76	67.93
0.33	0.13	0.53	47	84.56	66.90
0.44	0.11	0.44	45	87.71	63.79
0.56	0.09	0.36	42	88.85	63.45
0.67	0.07	0.27	38	92.34	59.31
0.78	0.04	0.18	32	100.79	52.07
0.89	0.02	0.09	21	143.13	32.76
1.00	0.00	0.00	0	∞	0.00

We reduce the grid cells to each size of 500 m^2. We find that in smaller cells, CPs are closer to each other, and thus, $d(i, j)$ between v_i and CP z_j is reduced. For instance, we evaluate the distribution of 81 CPs in $\mathcal{G}_{11}$ when the size is 1 km^2 and 500 m^2. Our results show that the mean distance reduces from 37.28 m to 22.67 m. Reducing the cell size facilitates a more granular distribution of CPs. By concentrating CPs in smaller grid cells, we increase proximity to EVs, making charging more accessible to users.

Table 10. Efficiency data with weights.

Weight w_t	Weight w_d	Weight w_p	Efficiency
0.00	0.20	0.80	0.4230
0.11	0.18	0.71	0.3937
0.22	0.16	0.62	0.3483
0.33	0.13	0.53	0.3161
0.44	0.11	0.44	0.3157
0.56	0.09	0.36	0.2378
0.67	0.07	0.27	0.2249
0.78	0.04	0.18	0.1910
0.89	0.02	0.09	0.1287

We calculate the efficiency as shown in Table 10 to understand how well CPs have been distributed in the simulation cell. By analysing $\eta[Y|w_t]$ for various values of w_t, w_d, and w_p in $\mathcal{G}_{11}$ selected for simulation, we find that the optimal weights for w_t, w_d, and w_p are 0.0, 0.2, and 0.8, respectively, and optimise the expected efficiency of the CP distribution. These set of weights produce an efficiency of 0.4229885.

Figure 17 shows how CPs are distributed in one of the cells in Dublin. Previously, research has used a variety of criteria, taking into account infrastructure to determine the ideal CP distribution. We extend the research in [13] by normalising parameter weights, rotating the grid, reducing the grid size to see the effect on CP distribution, and using a FNN to predict the best weight combination and the corresponding CP.

Figure 17. CPs distributed in a 1 km^2 cell in Dublin.

The results will help city planners and policymakers distribute resources for CP infrastructure. Policymakers can use the GEECharge method to identify the CP infrastructure needs of areas and maximise the benefit of infrastructure investment. Urban planners can use the findings to develop dynamic planning approaches that adapt to changes in traffic patterns and population growth. By optimising CP placement, cities can encourage more residents to adopt EVs, contributing to reduced emissions and promoting sustainable urban transportation. GEECharge can be adapted for use in other urban areas facing similar challenges with EV charging infrastructure as the parameters used are applicable in other cities. While this analysis is region-specific, GEECharge can be applied to other urban environments. Cities can use their local data in GEECharge by mapping data into a grid structure and feeding it into the FNN model for CP prediction. The flexibility of grid rotation allows for adapting to various urban layouts. Population density, traffic patterns, and POIs are relevant across urban contexts. The approach not only accommodates different urban layouts but is adaptable to diverse data. Future work could integrate energy supply capacities and infrastructure variations, as these factors could influence the distribution of CPs in different cities. This work leads to a successful CP distribution in Dublin that improves CP accessibility and lessens range anxiety.

This research is limited in that it can only identify CP placement locations. We have also not considered how the number of plugs for each CP could be adapted and the distance to the grid. Our research does not account for CP capacity, but future research could work on how each CP can handle multiple EVs at the same time. In Section 6 below, we have summarised the results and highlighted recommendations for future work.

6. Conclusions

The study provides valuable insights into optimising the distribution of CPs for EVs in urban environments. By normalising parameter weights and using FNN, we have identified the population density, points of interest, and most used road weights, such as optimal weights, grid resizing, and rotation angles, to maximise CP coverage while minimising MSE. We have also identified that summing all three weights to 1 ensures equity and balance in CP distribution contribution. We show that rotating the grid at $-350°$ increases the distribution of CPs by 5.7%. This will help address the current challenges facing EV adoption, particularly in urban areas where range anxiety and uneven CP distribution are significant concerns. Future research could explore additional factors, such as power distribution constraints and real-time demand fluctuations, to further refine CP placement strategies. Furthermore, integrating insights from EV user behaviour and preferences could enhance the effectiveness of CP networks, ensuring they are tailored to meet the needs of diverse user demographics and usage patterns.

Abbreviations

The following abbreviations are used in this manuscript:

GEECharge	Green Electric Charge
EV Portacharge	Electric Vehicle Portacharge
CP	Charging Point
DES	Discrete Event Simulation
POI	Point Of Interest
MAS	Multi-Agent System
MCDA	Multi-Criteria Decision Analysis
AHP	Analytical Hierarchy Process
MSE	Mean Squared Error
TOPSIS	Technique for Order Preference by Similarity to Ideal Solution
BESA	Bald Eagle Search Algorithm
ActBM	Activity-Based Micro-simulation model

References

1. Hao, H.; Cheng, X.; Liu, Z.; Zhao, F. Electric vehicles for greenhouse gas reduction in China: a cost-effectiveness analysis. *Transp. Res. Part D Transp. Environ.* **2017**, *56*, 68–84.
2. Kutlu, Y.; de Fréin, R.; Basu, M.; Malik, A. Round trip time measurement over microgrid power networks. In Proceedings of the IEEE Irish Signals and Systems Conference, Dublin, Ireland, 13–14 June 2023; pp. 1–6.
3. Board, E.S. Empowering Low-Carbon Living | ESB Annual Report. 2021. Available online: https://esb.ie/docs/default-source/investor-relations-documents/esb-annual-results-and-accounts-2021.pdf?sfvrsn=e43a00f0_2 (accessed on 20 March 2023).
4. KPMG. Ireland's 2030 Carbon Emissions Targets: An Economic Impact Assessment for the Agriculture Sector. 2021. Available online: https://assets.kpmg.com/content/dam/kpmg/ie/pdf/2021/11/ie-ireland-2030-carbon-emissions-targets.pdf/ (accessed on 20 March 2023).
5. Government, I. Climate Action Plan 2021: Securing Our Future. Available online: https://www.gov.ie/en/press-release/16421-climate-action-plan-2021-securing-our-future/ (accessed on 20 March 2023).
6. Bank, W. Electric Vehicles: An Economic and Environmental Win for Developing Countries. Available online: https://www.worldbank.org/en/news/feature/2022/11/17/electric-vehicles-an-economic-and-environmental-win-for-developing-countries/ (accessed on 19 May 2023).
7. Kene, R.; Olwal, T.; van Wyk, B.J. Sustainable electric vehicle transportation. *Sustainability* **2021**, *13*, 12379. https://doi.org/10.3390/su132212379.
8. ur Rehman, A.; Khalid, H.M.; Muyeen, S.M. Grid-integrated solutions for sustainable EV charging: A comparative study of renewable energy and battery storage systems. *Front. Energy Res.* **2024**, *12*, 1403883. https://doi.org/10.3389/fenrg.2024.1403883.

9. Khalid, H.M.; Flitti, F.; Muyeen, S.M.; Elmoursi, M.S.; Sweidan, T.O.; Yu, X. Parameter Estimation of Vehicle Batteries in V2G Systems: An Exogenous Function-Based Approach. *IEEE Trans. Ind. Electron.* **2022**, *69*, 9535–9546. https://doi.org/10.1109/TIE.2021.3112980.

10. Khalid, H.M.; Peng, J.C.H. Bidirectional Charging in V2G Systems: An In-Cell Variation Analysis of Vehicle Batteries. *IEEE Syst. J.* **2020**, *14*, 3665–3675. https://doi.org/10.1109/JSYST.2019.2958967.

11. Luo, C.; Huang, Y.F.; Gupta, V. Placement of EV charging stations—Balancing benefits among multiple entities. *IEEE Trans. Smart Grid* **2017**, *8*, 759–768. https://doi.org/10.1109/TSG.2015.2508740.

12. Mahdy, M.; Bahaj, A.S.; Turner, P.; Wise, N.; Alghamdi, A.S.; Hamwi, H. Multi criteria decision analysis to optimise siting of electric vehicle charging points: Case study Winchester District, UK. *Energies* **2022**, *15*, 2497.

13. Mutua, A.M.; de Fréin, R.; Ali, M.; Eliel, K.; Marco, S.; Maxime, P. Optimising electric vehicle charging infrastructure in Dublin using GEEcharge. In Proceedings of the EVI: Charging Ahead (EVI 2023), Glasgow, UK, 14 November–17 November 2023; Volume 2023, pp. 81–86. https://doi.org/10.1049/icp.2023.3130.

14. Martí, P.; Jordán, J.; Palanca, J.; Julian, V. Charging stations and mobility data generators for agent-based simulations. *Neurocomputing* **2022**, *484*, 196–210.

15. BU-1003a: Battery Aging in an Electric Vehicle (EV)-Battery University. Available online: https://batteryuniversity.com/article/bu-1003a-battery-aging-in-an-electric-vehicle-ev/ (accessed on 19 May 2023).

16. Steffen, T.; Fly, A.; Mitchell, W. Optimal electric vehicle charging considering the effects of a financial incentive on battery ageing. *Energies* **2020**, *13*, 4742. https://doi.org/10.3390/en13184742.

17. Nsaif, M.; Kovásznai, G.; Rácz, A.; Malik, A.; de Fréin, R. An adaptive routing framework for efficient power consumption in software-defined datacenter networks. *Electronics* **2021**, *10*, 3027. https://doi.org/10.3390/electronics10233027.

18. Sanguesa, J.A.; Torres-Sanz, V.; Garrido, P.; Martinez, F.J.; Marquez-Barja, J.M. A review on electric vehicles: technologies and challenges. *Smart Cities* **2021**, *4*, 372–404.

19. Khan, M.; Kar, N.C. Hybrid electric vehicles for sustainable transportation: a Canadian perspective. *World Electr. Veh. J.* **2009**, *3*, 551–562.

20. Babrowski, S.; Heinrichs, H.; Jochem, P.; Fichtner, W. Load shift potential of electric vehicles in Europe. *J. Power Sources* **2014**, *255*, 283–293.

21. Morrow, K.; Karner, D.; Francfort, J.E. *Plug-In Hybrid Electric Vehicle Charging Infrastructure Review*; U.S. Department of Energy: Washington, DC, USA, 2008

22. Volumes, E. Comparing EV Sales. 2024. Available online: https://ev-volumes.com// (accessed on 11 April 2024).

23. Technavio. EV Battery Market. 2024. Available online: https://www.technavio.com/report/electric-vehicle-battery-market-industry-size-analysis/ (accessed on 11 April 2024).

24. Statista. US EV Market. 2024. Available online: https://www.statista.com/outlook/mmo/electric-vehicles/united-states/ (accessed on 11 April 2024).

25. Agency, I.E. EV Sales Worldwide. 2024. Available online: https://www.iea.org// (accessed on 11 April 2024).

26. Coffman, M.; Bernstein, P.; Wee, S. Electric vehicles revisited: A review of factors that affect adoption. *Transp. Rev.* **2017**, *37*, 79–93. https://doi.org/10.1080/01441647.2016.1217282.

27. Hidrue, M.K.; Parsons, G.R.; Kempton, W.; Gardner, M.P. Willingness to pay for electric vehicles and their attributes. *Resour. Energy Econ.* **2011**, *33*, 686–705. https://doi.org/10.1016/j.reseneeco.2011.02.002.

28. Feng, J.; Khan, A.M. Accelerating urban road transportation electrification: planning, technology, economic and implementation factors in converting gas stations into fast charging stations. *Energy Syst.* **2024**. https://doi.org/10.1007/s12667-023-00638-4.

29. Schroeder, A.; Traber, T. The economics of fast charging infrastructure for electric vehicles. *Energy Policy* **2012**, *43*, 136–144. https://doi.org/10.1016/j.enpol.2011.12.041.

30. Madina, C.; Zamora, I.; Zabala, E. Methodology for assessing electric vehicle charging infrastructure business models. *Energy Policy* **2016**, *89*, 284–293. https://doi.org/10.1016/j.enpol.2015.12.007.

31. Wang, X.; Wang, J.; Xu, C.; Zhang, K.; Li, G. Electric Vehicle Charging Infrastructure Policy Analysis in China: A Framework of Policy Instrumentation and Industrial Chain. *Sustainability* **2023**, *15*, 2663. https://doi.org/10.3390/su15032663.

32. Engel, H.; Hensley, R.; Knupfer, S.; Sahdev, S. Charging ahead: Electric-vehicle infrastructure demand. *McKinsey Cent. Future Mobil.* **2018**, *8*, 1–8.

33. Ahn, Y.; Yeo, H. An analytical planning model to estimate the optimal density of charging stations for electric vehicles. *PLoS ONE* **2015**, *10*, e0141307. https://doi.org/10.1371/journal.pone.0141307.

34. Karolemeas, C.; Tsigdinos, S.; Tzouras, P.G.; Nikitas, A.; Bakogiannis, E. Determining electric vehicle charging station location suitability: A qualitative study of Greek stakeholders employing thematic analysis and analytical hierarchy process. *Sustainability* **2021**, *13*, 2298. https://doi.org/10.3390/su13042298.

35. Jordán, J.; Palanca, J.; del Val, E.; Julian, V.; Botti, V. Using genetic algorithms to optimize the location of electric vehicle charging stations. In Proceedings of the International Joint Conference SOCO'18-CISIS'18-ICEUTE'18, San Sebastián, Spain, 6–8 June 2018; Graña, M.; López-Guede, J.M.; Etxaniz, O.; Herrero, Á.; Sáez, J.A.; Quintián, H.; Corchado, E., Eds.; Springer: Cham, Switzerland, 2019; pp. 11–20.

36. Zhang, Y.; Liu, X.; Zhang, T.; Gu, Z. Review of the electric vehicle charging station location problem. In Proceedings of the International Conference on Dependability in Sensor, Cloud, and Big Data Systems and Applications, Guangzhou, China, 12–15 November 2019; Springer: Berlin/Heidelberg, Germany, 2019; pp. 435–445.

37. Hickerson, H.; Goldsmith, H.; Brazil, G.; Eckerle, V.T. *Electric Vehicle Charging Station Permitting Guidebook*, 2nd ed.; California Governor's Office of Business and Economic Development: Sacramento, CA, USA, 2023.

38. Government, I. Electric Vehicle Charging Infrastructure Strategy 2022–2025. 2023. Available online: https://www.gov.ie/transport/ (accessed on 22 April 2023).

39. Erbaş, M.; Kabak, M.; Özceylan, E.; Çetinkaya, C. Optimal siting of electric vehicle charging stations: A GIS-based fuzzy multi-criteria decision analysis. *Energy* **2018**, *163*, 1017–1031. https://doi.org/10.1016/j.energy.2018.08.140.

40. Tang, Z.; Guo, C.; Hou, P.; Fan, Y. Optimal siting of electric vehicle charging stations based on Voronoi diagram and FAHP method. *Energy Power Eng.* **2013**, *5*, 1404–1409. https://doi.org/10.4236/epe.2013.54b266.

41. Ge, S.; Feng, L.; Liu, H. The planning of electric vehicle charging station based on Grid partition method. In Proceedings of the 2011 International Conference on Electrical and Control Engineering, Yichang, China, 16–18 September 2011; pp. 2726–2730. https://doi.org/10.1109/ICECENG.2011.6057636.

42. González, J.; Alvaro, R.; Gamallo, C.; Fuentes, M.; Fraile-Ardanuy, J.; Knapen, L.; Janssens, D. Determining electric vehicle charging point locations considering drivers' daily activities. *Procedia Comput. Sci.* **2014**, *32*, 647–654. https://doi.org/10.1016/j.procs.2014.05.472.

43. de Fréin, R.; O'Farrell, L. Distance-based Cluster Head Election for Mobile Sensing. In Proceedings of the 2018 12th International Conference on Sensing Technology (ICST), Limerick, Ireland, 4–6 December 2018; pp. 196–201. https://doi.org/10.1109/ICSensT.2018.8603606.

44. Loomba, R.; de Fréin, R.; Jennings, B. Selecting Energy Efficient Cluster-Head Trajectories for Collaborative Mobile Sensing. In Proceedings of the 2015 IEEE Global Communications Conference (GLOBECOM), San Diego, CA, USA, 6–10 December 2015, pp. 1–7. https://doi.org/10.1109/GLOCOM.2015.7417727.

45. Hengsong, W.; Huang, Q.; Zhang, C.; Xia, A. A novel approach for the layout of electric vehicle charging station. In Proceedings of the 2010 International Conference on Apperceiving Computing and Intelligence Analysis Proceeding, Chengdu, China, 17–19 December 2010; pp. 64–70. https://doi.org/10.1109/ICACIA.2010.5709852.

46. Pallonetto, F.; Galvani, M.; Torti, A.; Vantini, S. A framework for analysis and expansion of public charging infrastructure under fast penetration of electric vehicles. *World Electr. Veh. J.* **2020**, *11*, 18.

47. Xi, X.; Sioshansi, R.; Marano, V. Simulation–optimization model for location of a public electric vehicle charging infrastructure. *Transp. Res. Part Transp. Environ.* **2013**, *22*, 60–69.

48. Ahmad, F.; Iqbal, A.; Ashraf, I.; Marzband, M.; Khan, I. Optimal location of electric vehicle charging station and its impact on distribution network: A review. *Energy Rep.* **2022**, *8*, 2314–2333. https://doi.org/10.1016/j.egyr.2022.01.180.

49. Woo, H.; Son, Y.; Cho, J.; Choi, S. Stochastic second-order conic programming for optimal sizing of distributed generator units and electric vehicle charging stations. *Sustainability* **2022**, *14*, 4964. https://doi.org/10.3390/su14094964.

50. Yuvaraj, T.; Devabalaji, K.R.; Kumar, J.A.; Thanikanti, S.B.; Nwulu, N. A comprehensive review and analysis of the allocation of electric vehicle charging stations in distribution networks. *IEEE Access* **2024**, *12*, **5404-5461.** . https://doi.org/10.1109/ACCESS.2023.3349274.

51. Wu, Y.; Lu, Y.; Zhu, Z.; Holguín-Veras, J. Optimizing electric vehicle charging infrastructure on highways: A multi-agent-based planning approach. *Sustainability* **2023**, *15*, 13634. https://doi.org/10.3390/su151813634.

52. Gagarin, A.; Corcoran, P. Multiple domination models for placement of electric vehicle charging stations in road networks. *Comput. Oper. Res.* **2018**, *96*, 69–79. https://doi.org/10.1016/j.cor.2018.03.014.

53. Bersani, C.; Zero, E.; Sacile, R. A decision support system for the optimal location of electric vehicle charging points. In Proceedings of the 2019 IEEE International Conference on Systems, Man and Cybernetics (SMC), Bari, Italy, 6–9 October 2019; pp. 2707–2712. https://doi.org/10.1109/SMC.2019.8914033.

54. Iqbal, S.; Alshammari, N.F.; Shouran, M.; Massoud, J. Smart and sustainable wireless electric vehicle charging strategy with renewable energy and internet of things integration. *Sustainability* **2024**, *16*, 2487. https://doi.org/10.3390/su16062487.

55. Guo, F.; Yang, J.; Lu, J. The battery charging station location problem: impact of users' range anxiety and distance convenience. *Transp. Res. Part Logist. Transp. Rev.* **2018**, *114*, 1–18.

56. Wu, Y.; Yang, M.; Zhang, H.; Chen, K.; Wang, Y. Optimal site selection of electric vehicle charging stations based on a cloud model and the PROMETHEE method. *Energies* **2016**, *9*, 157. https://doi.org/10.3390/en9030157.

57. Lam, A.Y.S.; Leung, Y.W.; Chu, X. Electric vehicle charging station placement: formulation, complexity, and solutions. *IEEE Trans. Smart Grid* **2014**, *5*, 2846–2856. https://doi.org/10.1109/TSG.2014.2344684.

58. Zhou, G.; Zhu, Z.; Luo, S. Location optimization of electric vehicle charging stations: Based on cost model and genetic algorithm. *Energy* **2022**, *247*, 123437. https://doi.org/10.1016/j.energy.2022.123437.

59. Li, L.; Li, Y.Q.; Yao, Y.H.; Ge, M. Layout planning of electric vehicle charging stations based on genetic algorithm. *East China Electr. Power* **2011**, *39*, 1004–1006.

60. Frade, I.; Ribeiro, A.; Gonçalves, G.; Antunes, A.P. Optimal location of charging stations for electric vehicles in a neighborhood in Lisbon, Portugal. *Transp. Res. Rec.* **2011**, *2252*, 91–98. https://doi.org/10.3141/2252-12.

61. Alanazi, F.; Alshammari, T.O.; Azam, A. Optimal charging station placement and scheduling for electric vehicles in smart cities. *Sustainability* **2023**, *15*, 16030. https://doi.org/10.3390/su152216030.

62. Chen, T.; Kockelman, K.; Khan, M. Locating electric vehicle charging stations. *Transp. Res. Rec.* **2013**, pp. 28–36. https://doi.org/10.3141/2385-04.

63. Ferro, G.; Minciardi, R.; Parodi, L.; Robba, M. Optimal planning of charging stations and electric vehicles traffic assignment: a bi-level approach. *IFAC-PapersOnLine* **2020**, *53*, 13275–13280. 21st IFAC World Congress, https://doi.org/https://doi.org/10.1016/j.ifacol.2020.12.157.

64. Zhang, H.; Shi, F. A multi-objective site selection of electric vehicle charging station based on NSGA-II. *Int. J. Ind. Eng. Comput.* **2024**, *15*, 293–306. https://doi.org/10.5267/j.ijiec.2023.9.009.

65. Kundu, A.; Feijoo, F.; Mesa, F.; Sankaranarayanan, S.; Aristizábal, A.J.; Castaneda, M. Power on the go: A solution to address electric vehicle charging challenges. *Mathematics* **2023**, *12*, 91. https://doi.org/10.3390/math12010091.

66. Ushijima-Mwesigwa, H.; Khan, M.Z.; Chowdhury, M.A.; Safro, I. Optimal installation for electric vehicle wireless charging lanes. *arXiv* **2017**, arXiv:1704.01022.

67. Gulbahar, I.T.; Sutcu, M.; Almomany, A.; Ibrahim, B.S.K.K. Optimizing electric vehicle charging station location on highways: A decision model for meeting intercity travel demand. *Sustainability* **2023**, *15*, 16716. https://doi.org/10.3390/su152416716.

68. Sweda, T.; Klabjan, D. An agent-based decision support system for electric vehicle charging infrastructure deployment. In Proceedings of the 2011 IEEE Vehicle Power and Propulsion Conference, Chicago, IL, USA, 6–9 September 2011.

69. He, F.; Wu, D.; Yin, Y.; Guan, Y. Optimal deployment of public charging stations for plug-in hybrid electric vehicles. *Transp. Res. Part Methodol.* **2013**, *47*, 87–101. https://doi.org/10.1016/j.trb.2012.09.007.

70. Dong, X.; Mu, Y.; Jia, H.; Wu, J.; Yu, X. Planning of fast EV charging stations on a round freeway. *IEEE Trans. Sustain. Energy* **2016**, *7*, 1452–1461. https://doi.org/10.1109/TSTE.2016.2547891.

71. Worley, O.; Klabjan, D.; Sweda, T.M. Simultaneous vehicle routing and charging station siting for commercial electric vehicles. In Proceedings of the 2012 IEEE International Electric Vehicle Conference, Greenville, SC, USA, 4–8 March 2012; pp. 1–3.

72. Parent, P.L.; Carvalho, M.; Anjos, M.F.; Atallah, R. Maximum flow-based formulation for the optimal location of electric vehicle charging stations. *arXiv* **2023**, arXiv:2312.05980.

73. Statista. Population of Seoul. Available online: https://www.statista.com/statistics/756290/south-korea-population-of-seoul// (accessed on 8 May 2024).

74. World population review. Population of Chengdu, China. Available online: https://worldpopulationreview.com/world-cities/chengdu-population/ (accessed on 14 May 2024).

75. Statista. Population of Beijing. Available online: https://www.statista.com/statistics/1137629/china-population-of-beijing-municipality-administrative-area// (accessed on 8 May 2024).

76. Statista. Population of Hainan, Island. Available online: https://www.statista.com/statistics/1391706/china-population-of-hainan-province// (accessed on: 14 May 2024).

77. World Population Review. Population of Ireland. Available online: https://worldpopulationreview.com/countries/ireland-population/ (accessed on: 14 May 2024).

78. Microtrends. Population of Hohhot. Available online: https://www.macrotrends.net/global-metrics/cities/20551/hohhot/population#:~:text=The%20current%20metro%20area%20population,a%203.26%25%20increase%20from%202021./ (accessed on 8 May 2024).

79. World population review. Population of Valencia. Available online: https://worldpopulationreview.com/world-cities/valencia-population/ (accessed on 8 May 2024).

80. Cubit planning. Population of Chicagoland area. Available online: https://www.illinois-demographics.com/counties_by_population/ (accessed on 8 May 2024).

81. USA Government census data 2023 estimates. Population of Boston, USA. Available online: https://data.census.gov/profile?q=boston/ (accessed on 16 October 2024).

82. USA Government census data 2023 estimates. Population of Dublin, USA. Available online: https://data.census.gov/profile?q=dublin (accessed on 16 October 2024).

83. Infoplease. Population of Texas, New York and California. Available online: https://www.infoplease.com/us/states/state-population-by-rank/ (accessed on 14 May 2024).

84. World population review. Population of Ankara, Turkey. Available online: https://worldpopulationreview.com/world-cities/ankara-population/ (accessed on 14 May 2024).

85. World population review. Population of Winchester. Available online: https://worldpopulationreview.com/world-cities/winchester-population/ (accessed on 14 May 2024).

86. Statistiek Vlaanderen. Population of Flanders Region. Available online: https://www.statista.com/statistics/517196/population-of-belgium-by-region// (accessed on 8 November 2024).

87. Macrotrends. Population of Hong Kong. Available online: https://www.macrotrends.net/global-metrics/countries/HKG/hong-kong/population/ (accessed on 14 May 2024).

88. Microtrends. Population of Lisbon. Available online: https://www.macrotrends.net/global-metrics/cities/22167/lisbon/population/ (accessed on 8 May 2024).

89. Government, I. Traffic Flow Data. 2021. Available online: https://data.gov.ie/ (accessed on 28 October 2022).

90. Nakahara, M. *Geometry, Topology, and Physics*; Institute of Physics Publishing: Bristol, UK, 2005; p. 573.
91. Strang, G. *Linear Algebra and Its Applications*, 4th ed.; Jones & Bartlett Publishers: Burlington, MA, USA, 2012.
92. van Raan, A.F. German cities with universities: Socioeconomic position and university performance. *Quant. Sci. Stud.* **2022**, *3*, 265–288.
93. Michelin, V. Traffic Information Ireland. 2024. Available online: https://www.viamichelin.com/web/Traffic/Traffic-info-Ireland/ (accessed on 11 April 2024).
94. EVdatabase. Compare Electric Vehicles. 2022. Available online: https://ev-database.org/ (accessed on 30 January 2023).